Quantum electronics

12

Spin devices II

Maciej Urbaniak

IFM PAN

Politechnika Poznańska 2017

Spin devices II

- Magnetic semiconductors
- Spin injection
- Spin transistors

IFM PAN
Maciej Urbaniak
Politechnika Poznańska 2017

Energy bands in various types of materials

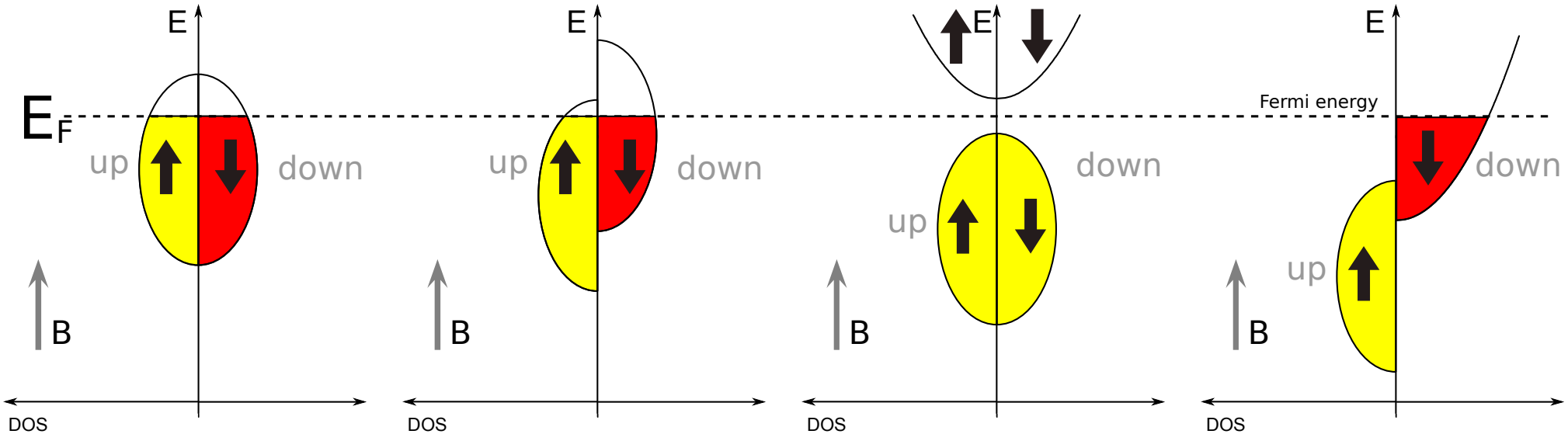

normal metal | ferromagnet | semiconductor | half-metal

Ferromagnetic (or ferrimagnetic etc.) properties are usually associated with transition metals **Fe, Co, Ni** and their alloys/compounds.
The family of compounds XYZ (half-Heusler) or X_2YZ (**full-Heusler**) with X,Y typically transition metals and Z main group element can be tailored to show ferromagnetism, superconductivity or insulating properties [3]. Some of Heusler compounds display half-metallicity with potential for applications in **spintronics**.
Spin polarization of a material:

$$P_0 = \frac{N_\uparrow - N_\downarrow}{N_\uparrow + N_\downarrow}, \qquad N_\uparrow, N_\downarrow - \text{density of states, at Fermi energy, for majority/minority electrons}$$

In 3d ferromagnets the positive spin polarization is associated with more mobile 4s electrons which are polarized by hybridization with 3d states [4]

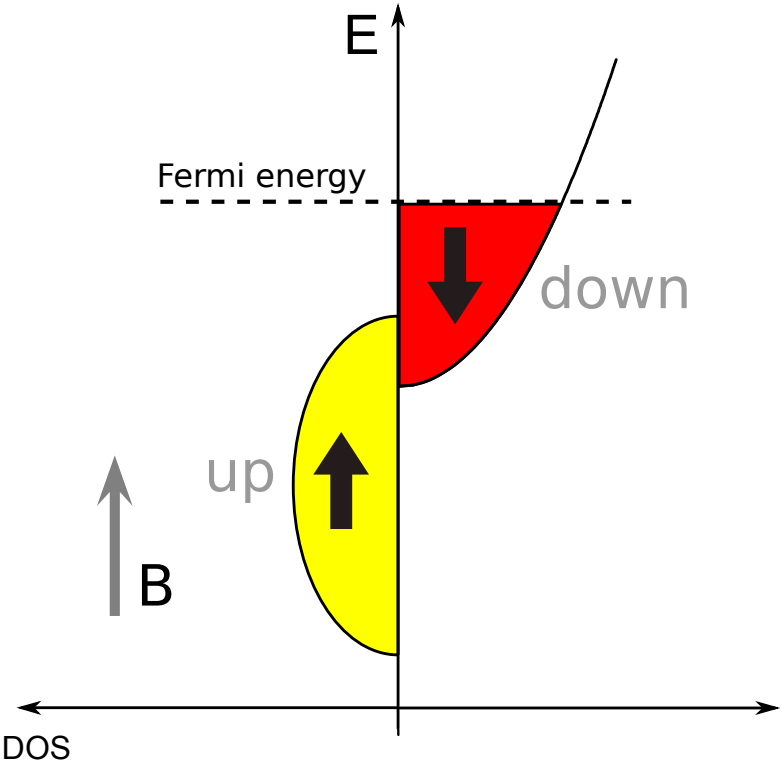

- NiMnSb, $NiMnV_2$ [4], Mn_2VAl, Co_2TiSn, Co_2FeSi [5] etc. - half metallic Heusler compounds
- Heuslers are attractive because of their relatively high Curie temperature in relation to other half-metals [5]
- Half-metals can be considers hybrid between metals and semiconductors – electrons with one spin display metallic behavior the others act like in a semiconductor [5]

Giant TMR - example

The highest amplitude to-day tunneling magnetoresistance amplitude was obtained using half metallic Heusler Co_2MnSi compound

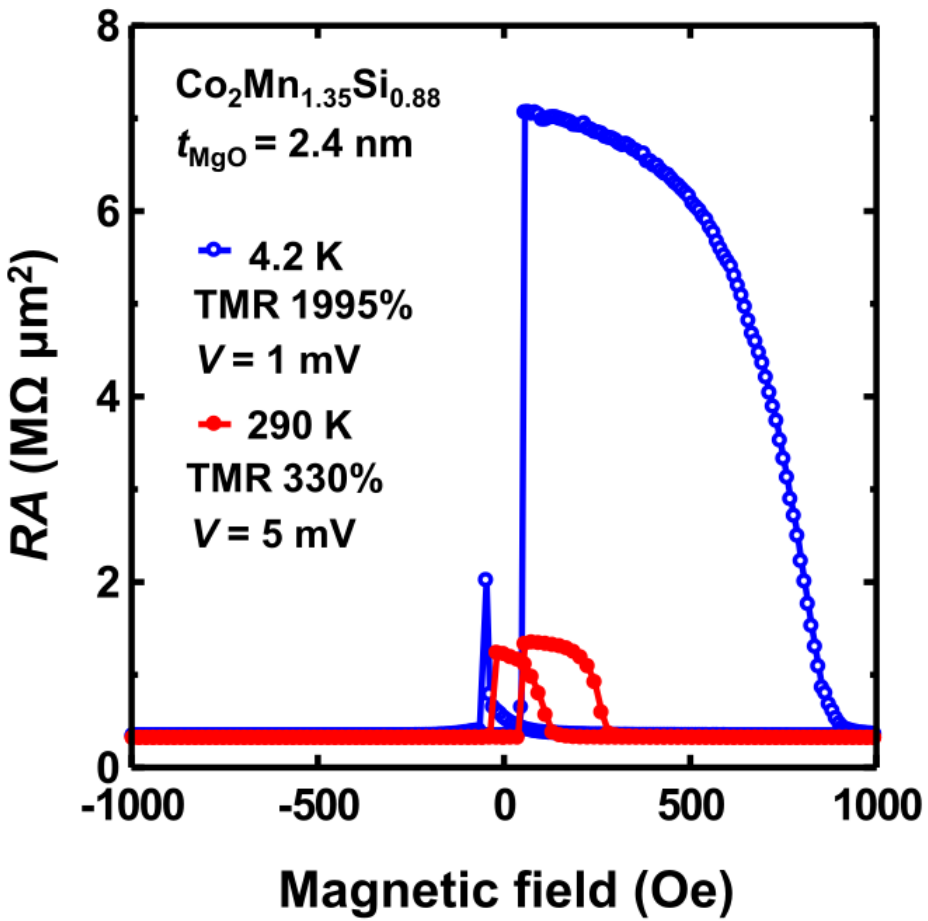

FIG. 2. Typical TMR curves at 4.2 K and 290 K for a Co_2MnSi MTJ consisting of (from the lower side) Co_2MnSi lower electrode (3 nm)/MgO barrier (2.4 nm)/Co_2MnSi upper electrode (3 nm) grown on a CoFe-buffered MgO(001) substrate with Mn-rich $Co_2Mn_{1.35}Si_{0.88}$ electrodes (MTJ-B). The magnetoresistance was measured with a magnetic field applied along the [1-10] axis of the Co_2MnSi film using a dc four-probe method. The bias voltages were 1 mV at 4.2 K and 5 mV at 290 K.

- MgO(001)/MgO(10nm)/CoFe(30nm)/Co_2MnSi/MgO/Co_2MnSi

  MgO buffered MgO(001) – MgO deposited on MgO crystal

- T_c = 985K
- room temperature (290K) **TMR≈340%**

Compare with *old* "metallic" TMR:

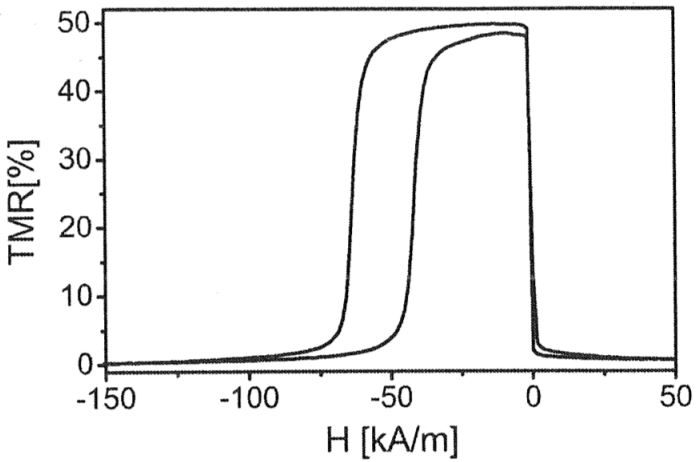

Fig. 6 The room temperature TMR curve of Cu(30 nm)/$Ni_{80}Fe_{20}$(4 nm)/$Mn_{83}Ir_{17}$(15 nm)/$Co_{70}Fe_{30}$ (2 nm)/Al(1.4 nm) + Ox/$Ni_{80}Fe_{20}$(4 nm)/Ta(3 nm)/ Cu(55 nm)/Au (20 nm) multilayer.

image from: M. Urbaniak *et al.*, Physica Status Solidi A **199**, 284 (2003)

image from: H-Xi. Liu , Y. Honda, T. Taira , K-ichi. Matsuda , M. Arita , T. Uemura, M. Yamamoto, Appl. Phys. Lett. **101**, 132418 (2012) [7]

There is an ongoing search for materials displaying both magnetic and semiconductor properties.
Most magnetically doped semiconductors and semiconductor oxides, that display ferromagnetic features, can be grouped into two main classes [1]:

- **uniform systems** with randomly distributed transition metals cations (Mn,Fe,Co,Ni) where spin-spin interactions are mediated by holes [eg. (Ga,Mn)As]

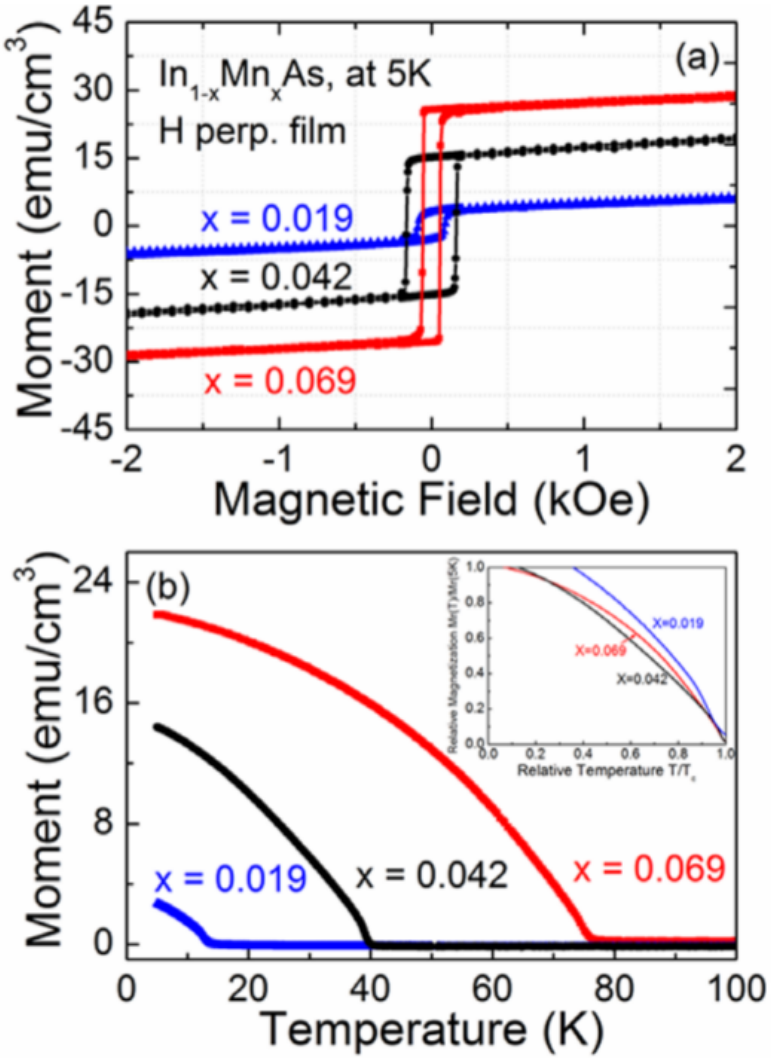

- $In_{1-x}Mn_xAs$ epilayers [2]
- Mn implantation (100keV) followed by pulsed laser melting on InAs (001) substrates
- **ferromagnetism**, low saturation field, T_c=82K at x=0.105
- perpendicular magnetic anisotropy (field parallel to [001] axis) – due to strain induced by the Mn ion substitution

image from: Y. Yuan *et al.*, Journal of Physics D Applied Physics **48**, 235002 (2015) [2]

Figure 1. (a) Magnetization of $In_{1-x}Mn_xAs$ samples measured at 5 K in the out-of-plane geometry: the Mn concentrations are: x = 0.019 (triangle), 0.042 (circle) and 0.069 (square); (b) remanent magnetization as a function of temperature measured under a magnetic field of 20 Oe after the samples were saturated by applying 1000 Oe along the perpendicular direction for the three samples. The inset shows the plots of Mr(T)/Mr(5 K) as a function of T/T_C.

Diluted magnetic semiconductors

There is an ongoing search for materials displaying both magnetic and semiconductor properties.
Most magnetically doped semiconductors and semiconductor oxides, that display ferromagnetic features, can be grouped into two main classes [1]:

- **heterogeneous systems** with non-random distribution of magnetic elements – ferromagnetic-like properties are determined by **nanoregions** with high concentration of magnetic cations

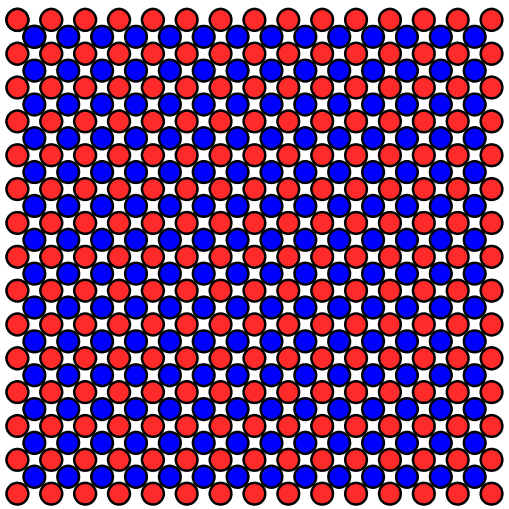

chemical phase separation
(spinodal decomposition)

for examples see A. Bonani *et al.*[9]

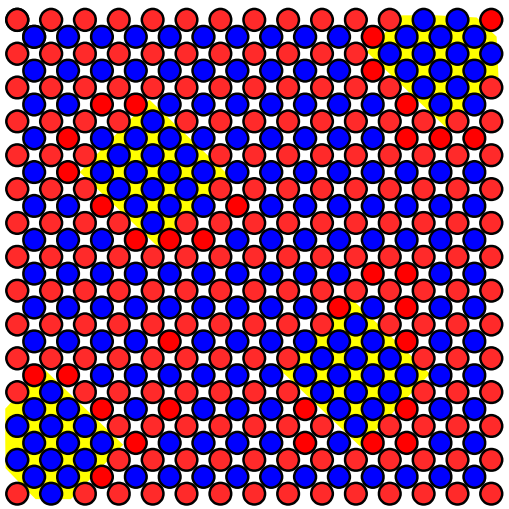

"*The element-semiconductors silicon and germanium are widely used, but nowadays binary, ternary, and even quaternary semi- conductors such as GaN,$GaP_{1-x}As_x$, or $Cu(GaIn)Se_2$ play an important role in electronics and materials for energy conversion. More elements allow for more degrees of freedom such as band-gap tuning and multi-functionality.*" - C. Felser et al.

- an unpolarized current (both spin channels carrying equal current) is flowing under the action of an **E**elecrto**M**otoric**F**orce into left ferromagnet (electrode, LE)
- the current experiences polarization and enters the middle, non-ferromagnetic (NM) conductor
- the surplus spin is not dissipated at once but increases magnetic moment at the interface – **spin accumulation** [10]. Its extent is determined by an *equilibrium* between spin injection rate and spin-flip rate in NM

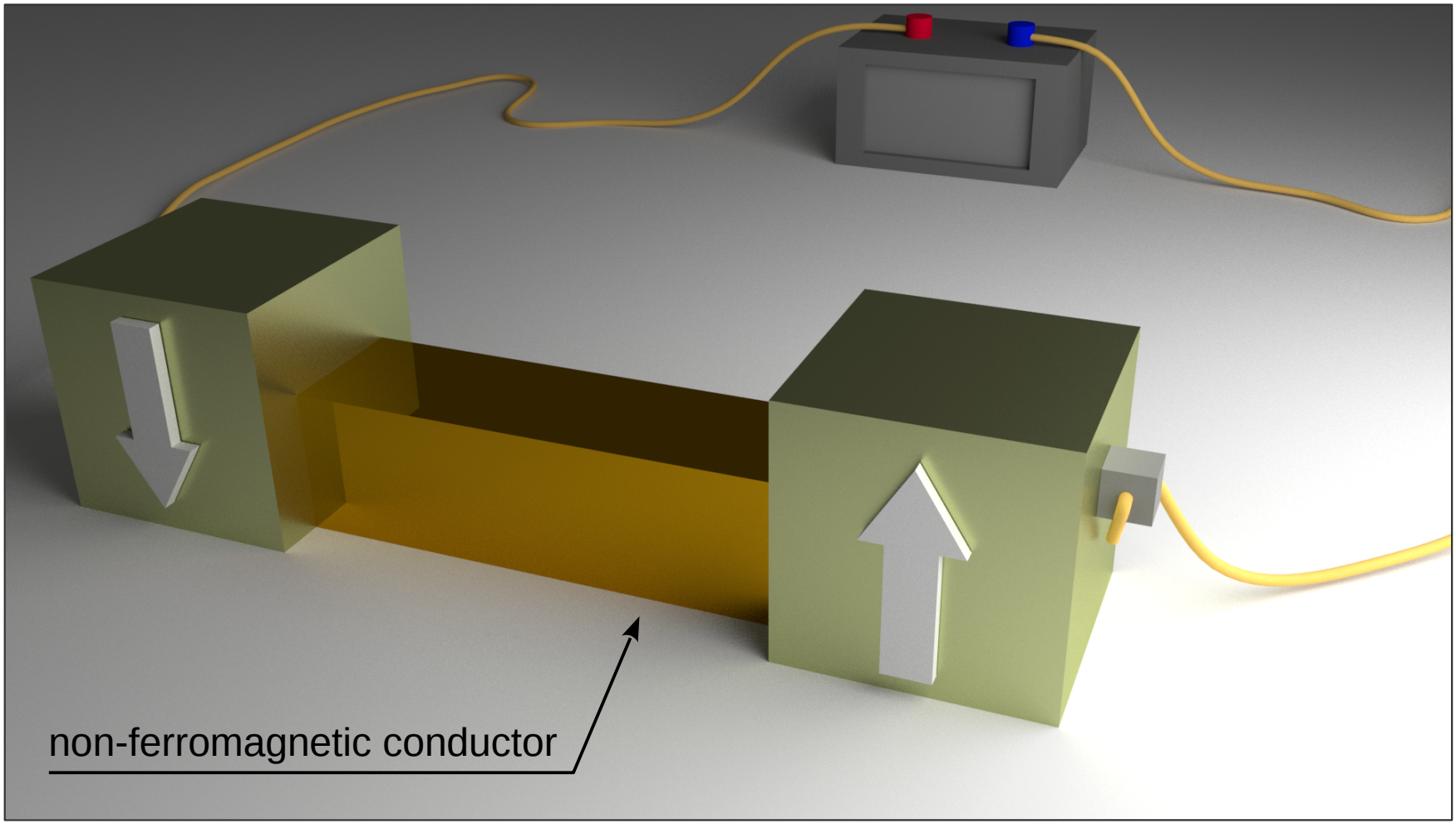

- an unpolarized current (both spin channels carrying equal current) is flowing under the action of an **E**elecrto**M**otoric**F**orce into left ferromagnet (electrode, LE)
- the current experiences polarization and enters the middle, non-ferromagnetic (NM) conductor
- the surplus spin is not dissipated at once but increases magnetic moment at the interface – **spin accumulation** [10]. Its extent is determined by an *equilibrium* between spin injection rate and spin-flip rate in NM
- the spins injected into NM experience scattering and after some time $\tau_{\uparrow\downarrow}$, on average their magnetization is zero. They travel in that time a **spin diffusion length**

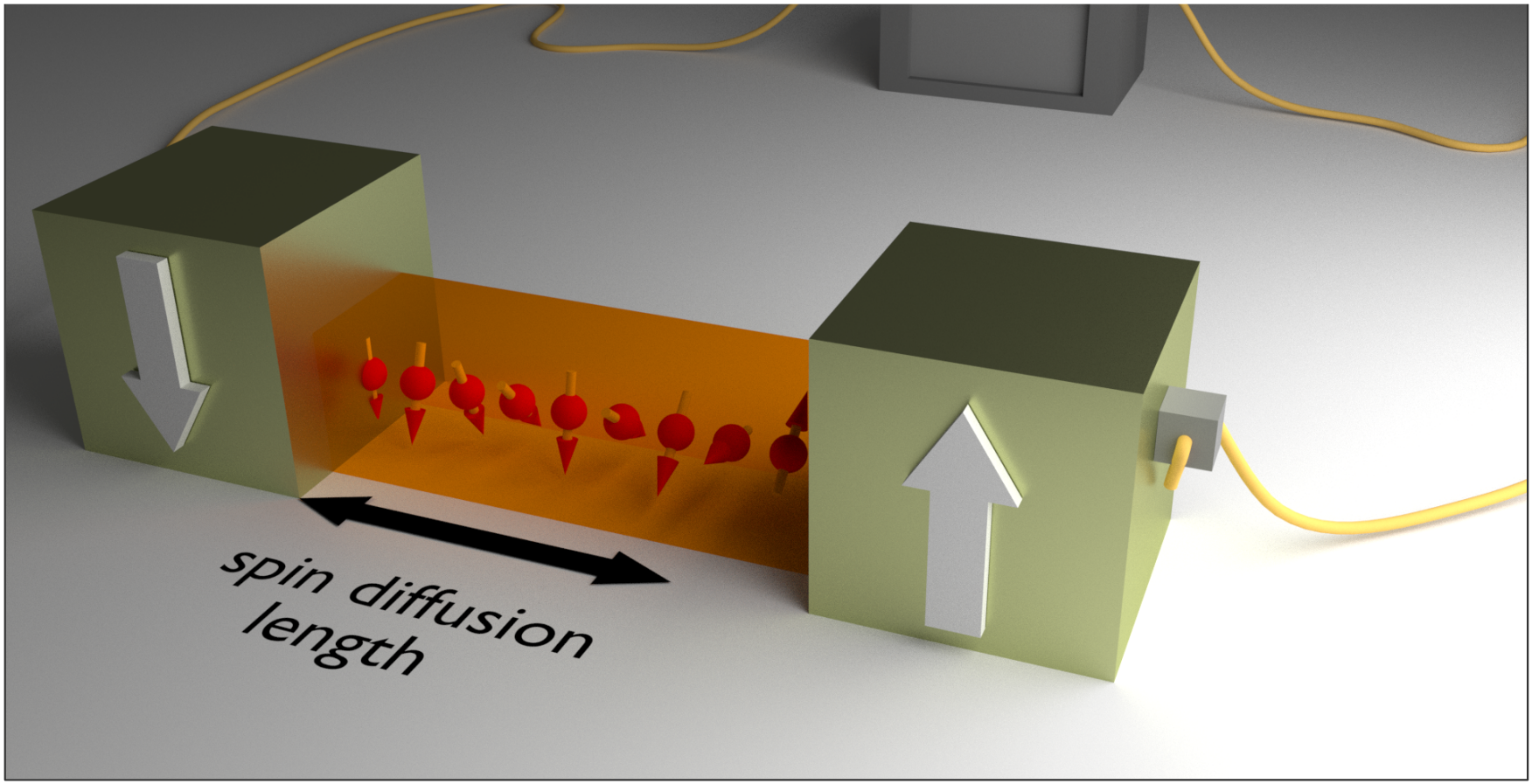

- an unpolarized current (both spin channels carrying equal current) is flowing under the action of an **E**elecrto**M**otoric**F**orce into left ferromagnet (electrode, LE)
- the current experiences polarization and enters the middle, non-ferromagnetic (NM) conductor
- the surplus spin is not dissipated at once but increases magnetic moment at the interface – **spin accumulation** [10]. Its extent is determined by an *equilibrium* between spin injection rate and spin-flip rate in NM
- the spins injected into NM experience scattering and after some time $\tau_{\uparrow\downarrow}$, on average their magnetization is zero. They travel in that time a **spin diffusion length**
- only if spin diffusion length is longer than the conductor connecting the ferromagnetic electrodes the magnetic state of the left electrode can influence the state of right one

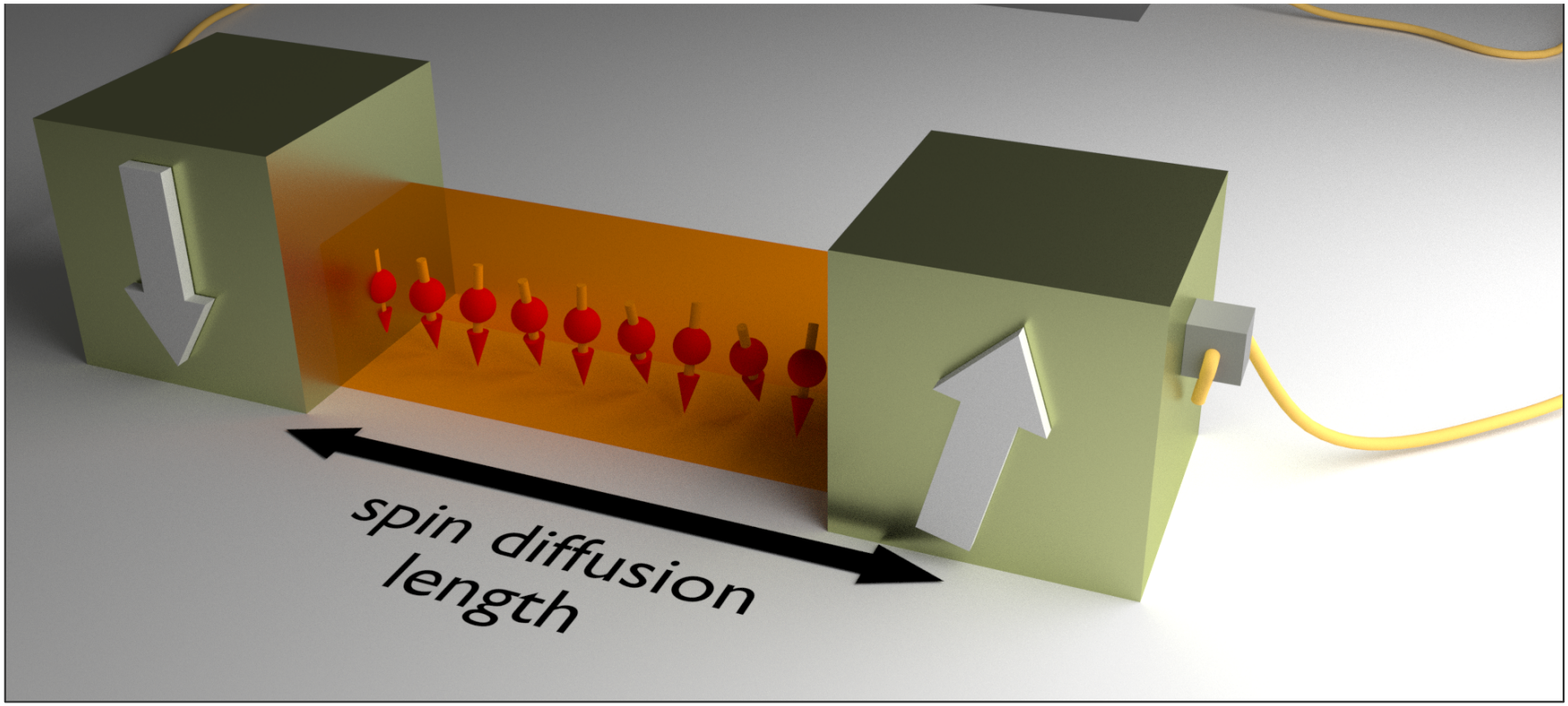

Einstein relation*

Consider electron gas at 0K: drift current and diffusion currents at steady state must be equal [11]. We have then

$$\vec{j}_e+\vec{j}_D=\sigma\vec{E}+eD\nabla n, \qquad D\text{-diffusion constant}, \quad n\text{-particle density } [m^{-3}],\ \sigma\text{-conductivity} \qquad (1)$$

Electrochemical potential is defined as

$\mu=-eV+E_F$ and its gradient can be written as

$$D(E_F)=\left(\frac{dn}{dE}\right)_{E_F} \rightarrow \frac{dE_F}{dn}=\frac{1}{D(E_F)}$$

$$\nabla\mu=e\vec{E}+\nabla E_F=e\vec{E}+\frac{dE_F}{dn}\nabla n=e\vec{E}+\frac{1}{D(E_F)}\nabla n$$

inserting gradient of n (Eq.1) into the above equation gives

$$\nabla\mu=e\vec{E}-\frac{1}{D(E_F)}\frac{\sigma\vec{E}}{De}=\left(e-\frac{1}{D(E_F)}\frac{\sigma}{De}\right)\vec{E}$$

$$\nabla\mu=0$$

Because electrochemical potential is spatially constant at thermal equilibrium [11] and ***E*** is arbitrary we get*

$$\boxed{\sigma=e^2D(E_F)D}$$

$$\mu_B=\left(\frac{\partial G}{\partial n_B}\right)_{t,p,n_{X\neq B}}$$

$G=U-TS+pV$ -Gibbs energy;
formerly free energy or free enthalpy [13]

$\vec{j}=-D\nabla n$-Fick's first law

*for electrons. Classical Einstein relations for Brownian motion at equilibrium relates proportionality factor between terminal velocity under the action of force in viscous liquid and that force with diffusion constant [12]

We analyze separately both spin channels (↑ and ↓). The current density is proportional to a gradient of the electrochemical potential:

$$\frac{\partial \mu^{\uparrow,\downarrow}}{\partial x} = \frac{-e\, j^{\uparrow,\downarrow}}{\sigma^{\uparrow,\downarrow}} \qquad \vec{j}_e = \sigma \vec{E} \;\rightarrow\; \vec{E} = \frac{j_e}{\sigma} \;\rightarrow\; \text{electric force: } \vec{F}_e = e\vec{E} = \frac{e\, j_e}{\sigma}, \quad -\frac{\partial \mu^{\uparrow,\downarrow}}{\partial x} = \text{force} \qquad (2)$$

The spin diffusion equation, in 1D, reads (this comes from the second Fick's law)

$$\frac{\partial C}{\partial t} = D \nabla^2 C$$

C-concentration

$$\frac{\mu^{\uparrow} - \mu^{\downarrow}}{\tau_{sf}} = D \frac{\partial^2 (\mu^{\uparrow} - \mu^{\downarrow})}{\partial x^2}$$

this is written in a relaxation time approximation - $\tau_{\uparrow\downarrow}$ determines the return to equilibrium

The general solution of the above equation is

$$\mu^{\uparrow} - \mu^{\downarrow} = C_1(t)\, e^{\frac{x}{\sqrt{D\tau_{sf}}}} + C_2(t)\, e^{-\frac{x}{\sqrt{D\tau_{sf}}}}, \quad \text{where } \sqrt{D\tau_{sf}} \text{ is a spin diffusion length}$$

- **Spin diffusion length** is a typical length scale on which the spin information is lost

Exemplary solution of diffusion equation for a constant concentration of diffusing species at x=0 [14] – complementary error function:

$$c(x,t) = C_s\, erfc\left(\frac{x}{2\sqrt{Dt}}\right)$$

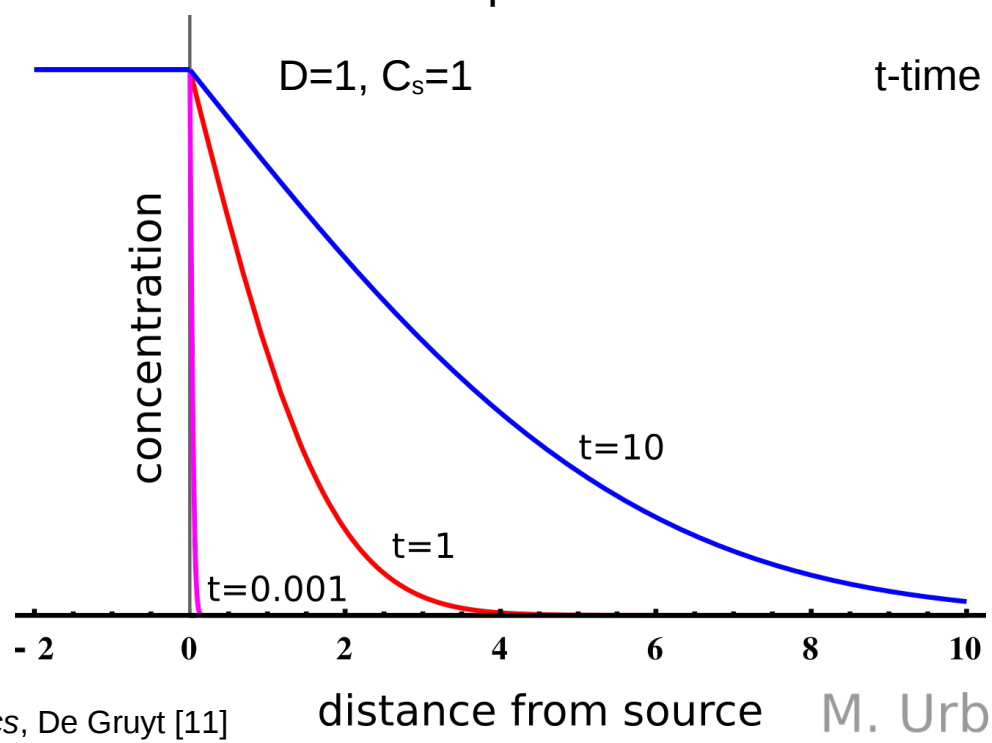

*the derivation follows T. Schäpers *Semiconductor Spintronics*, De Gruyt [11]

The expression for the spin polarization, using the Einstein relation, can be written as

$$\beta=\frac{\sigma_{FM}^{\uparrow}-\sigma_{FM}^{\downarrow}}{\sigma_{FM}^{\uparrow}+\sigma_{FM}^{\downarrow}}$$

$$\sigma=e^2 D(E_F) D \qquad P_0,\beta=\frac{N_{\uparrow}-N_{\downarrow}}{N_{\uparrow}+N_{\downarrow}}=\frac{D_{\uparrow}(E_F)-D_{\downarrow}(E_F)}{D_{\uparrow}(E_F)+D_{\downarrow}(E_F)}$$

In non-ferromagnetic semiconductor the conductivity does not depend on spin

$$\sigma_{SC}^{\uparrow,\downarrow}=\frac{1}{2}\sigma_{SC} \quad \rightarrow \quad \beta=0$$

We want to find the profile of the electrochemical potential in the vicinity of the ferromagnet/ semiconductor interface. The general solutions of the diffusion equation are [11]

$$\mu^{\uparrow,\downarrow}(x)=\mu_0^{FM}+a\,x+c^{\uparrow,\downarrow}e^{x/\lambda_{FM}} \qquad \text{for } x\leq 0$$

$$\mu^{\uparrow,\downarrow}(x)=\mu_0^{SC}+b\,x+d^{\uparrow,\downarrow}e^{-x/\lambda_{SC}} \qquad \text{for } x>0$$

$$\lambda_{sf}=\sqrt{D\tau_{sf}} \qquad \frac{\mu^{\uparrow}-\mu^{\downarrow}}{\lambda_{sf}^2}=\frac{\partial^2(\mu^{\uparrow}-\mu^{\downarrow})}{\partial x^2}$$

In order to fit both μ dependences at the interface it suffices to have **one offset** coefficient

$$\mu_0^{FM}=0$$

$$\mu_0^{SC} \rightarrow \boxed{\mu_{\text{off(set)}}}$$

The relation between both *c* coefficients can be found from current conservation - the total current must be constant: $j(x)=j^{\uparrow}(x)+j^{\downarrow}(x)=const$

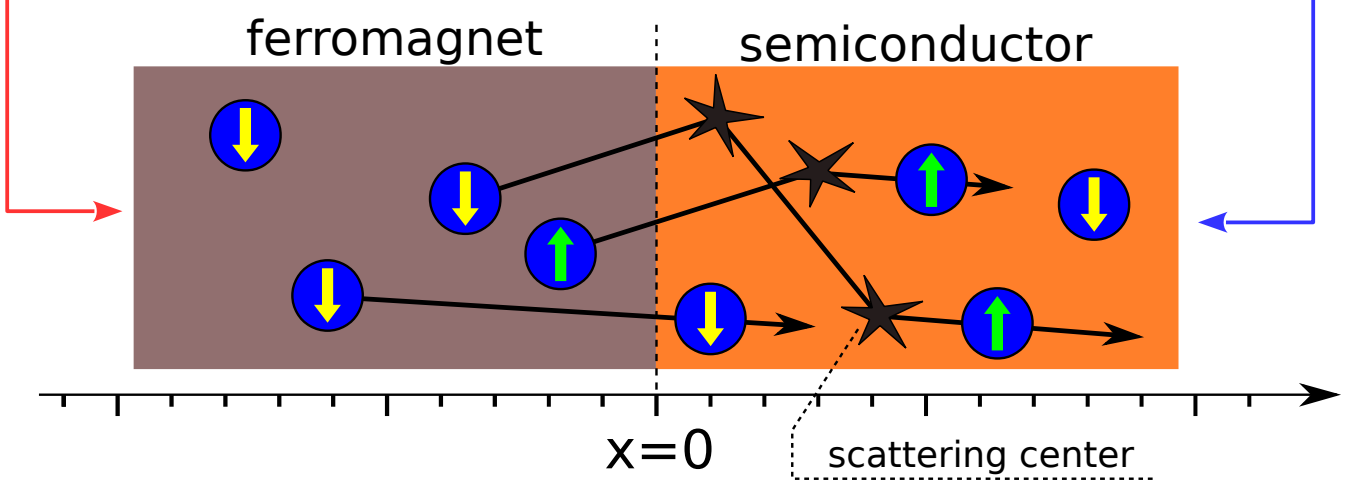

We obtain the current density inserting the solution for the ferromagnet into equation (2)

$$j^{\uparrow,\downarrow}=-\frac{\sigma_{FM}^{\uparrow,\downarrow}}{e}\frac{\partial\mu^{\uparrow,\downarrow}}{\partial x}=-\frac{\sigma_{FM}^{\uparrow,\downarrow}}{e}\left(a+\frac{c^{\uparrow,\downarrow}}{\lambda_{FM}}e^{x/\lambda_{FM}}\right)$$

$$\frac{\partial\mu^{\uparrow,\downarrow}}{\partial x}=\frac{-e\,j^{\uparrow,\downarrow}}{\sigma^{\uparrow,\downarrow}} \leftarrow \mu^{\uparrow,\downarrow}(x)=a\,x+c^{\uparrow,\downarrow}e^{x/\lambda_{FM}}$$

We assume that the total current density at x=-∞ and at x=0 is the same. We have then

$$j(-\infty)=j^{\uparrow}(-\infty)+j^{\downarrow}(-\infty)=-\frac{\sigma_{FM}^{\uparrow}}{e}(a+0)-\frac{\sigma_{FM}^{\downarrow}}{e}(a+0)$$

$$j(0)=j^{\uparrow}(0)+j^{\downarrow}(0)=-\frac{\sigma_{FM}^{\uparrow}}{e}\left(a+\frac{c^{\uparrow}}{\lambda_{FM}}\right)-\frac{\sigma_{FM}^{\downarrow}}{e}\left(a+\frac{c^{\downarrow}}{\lambda_{FM}}\right)$$

Equating both currents we get

$$\frac{\sigma_{FM}^{\uparrow}}{e}\frac{c^{\uparrow}}{\lambda_{FM}}+\frac{\sigma_{FM}^{\downarrow}}{e}\frac{c^{\downarrow}}{\lambda_{FM}}=0 \rightarrow \boxed{c^{\uparrow}=-c^{\downarrow}\frac{\sigma_{FM}^{\downarrow}}{\sigma_{FM}^{\uparrow}}}$$

We assume that spin-diffusion length in ferromagnet is the same for both spin channels

Analogous calculations can be performed for semiconductor side (x>0) and since both spin channels have equal conductivity we have

$$d^{\uparrow}=-d^{\downarrow}\frac{\sigma_{SM}^{\downarrow}}{\sigma_{SM}^{\uparrow}}=-d^{\downarrow}\frac{\sigma_{SM}/2}{\sigma_{SM}/2} \rightarrow \boxed{d^{\uparrow}=-d^{\downarrow}}$$

$$\sigma_{SC}^{\uparrow,\downarrow}=\frac{1}{2}\sigma_{SC}$$

The electrochemical potential is continuous everywhere, and in particular at x=0:

$$\mu_{FM}^{\uparrow,\downarrow}(0)=\mu_{SC}^{\uparrow,\downarrow}(0) \Rightarrow \begin{array}{ll}\mu_{FM}^{\uparrow}(0)=\mu_{SC}^{\uparrow}(0): & c^{\uparrow}=\mu_{off}+d^{\uparrow}\\ \mu_{FM}^{\downarrow}(0)=\mu_{SC}^{\downarrow}(0): & c^{\downarrow}=\mu_{off}+d^{\downarrow}\end{array}$$

$$\mu^{\uparrow,\downarrow}(x)=a\,x+c^{\uparrow,\downarrow}e^{x/\lambda_{FM}} \quad \text{for } x\le 0$$

$$\mu^{\uparrow,\downarrow}(x)=\mu_{off}+b\,x+d^{\uparrow,\downarrow}e^{-x/\lambda_{SC}} \quad \text{for } x>0$$

The coefficients d and μ_{off} are thus given by

$$\boxed{\mu_{off}=\frac{c^{\uparrow}+c^{\downarrow}}{2} \qquad d^{\uparrow}=\frac{c^{\uparrow}-c^{\downarrow}}{2}}$$

$$d^{\uparrow}=-d^{\downarrow} \qquad c^{\uparrow}=\mu_{off}+d^{\uparrow} \qquad c^{\downarrow}=\mu_{off}+d^{\downarrow}$$

From the limits x=-∞ and x=∞, for ferromagnet and semiconductor respectively, we obtain

$$j^{\uparrow,\downarrow}=-\frac{\sigma^{\uparrow,\downarrow}}{e}\frac{\partial\mu^{\uparrow,\downarrow}}{\partial x} \qquad (2)$$

$$j_{FM}(-\infty)=j_{FM}^{\uparrow}(-\infty)+j_{FM}^{\downarrow}(-\infty)=-\frac{(\sigma_{FM}^{\uparrow}+\sigma_{FM}^{\downarrow})a}{e}=-\frac{\sigma_{FM}a}{e}$$

$$j_{SC}(+\infty)=j_{SC}^{\uparrow}(+\infty)+j_{SC}^{\downarrow}(+\infty)=-\frac{(\sigma_{SC}^{\uparrow}+\sigma_{SC}^{\downarrow})b}{e}=-\frac{\sigma_{SC}b}{e}$$

and since $j_{FM}(-\infty)=j_{SC}(+\infty):=j$ we have $\boxed{a=-\frac{e\,j}{\sigma_{FM}} \qquad b=-\frac{e\,j}{\sigma_{SC}}}$

From the continuity of up current at x=0 we get

$$j^{\uparrow}(0)_{FM}=-\frac{\sigma_{FM}^{\uparrow}}{e}\left(a+\frac{c^{\uparrow}}{\lambda_{FM}}\right)=-\frac{\sigma_{SC}/2}{e}\left(b-\frac{d^{\uparrow}}{\lambda_{SC}}\right)=j^{\uparrow}(0)_{SC}$$

which transforms to

$$c^{\uparrow}=-c^{\downarrow}\frac{\sigma_{FM}^{\downarrow}}{\sigma_{FM}^{\uparrow}}$$

$$-\frac{\sigma_{FM}^{\uparrow}}{e}\left(a+\frac{c^{\uparrow}}{\lambda_{FM}}\right)=-\frac{\sigma_{SC}/2}{e}\left(b-\left(\frac{c^{\uparrow}-c^{\downarrow}}{2}\right)\frac{1}{\lambda_{SC}}\right) \rightarrow \frac{\sigma_{FM}^{\uparrow}}{e}\left(a+\frac{c^{\uparrow}}{\lambda_{FM}}\right)=\frac{\sigma_{SC}}{2e}\left(b-c^{\uparrow}\left(1+\frac{\sigma_{FM}^{\downarrow}}{\sigma_{FM}^{\uparrow}}\right)\frac{1}{2\lambda_{SC}}\right)$$

Using expressions for *a* and *b* we can relate the above equation entirely to properties of the system (i.e. without arbitrary constants)

$$\frac{\sigma_{FM}^{\uparrow}}{e}\left(-\frac{e\,j}{\sigma_{FM}}+\frac{c^{\uparrow}}{\lambda_{FM}}\right)=\frac{\sigma_{SC}}{2e}\left(-\frac{e\,j}{\sigma_{SC}}-c^{\uparrow}\left(1+\frac{\sigma_{FM}^{\downarrow}}{\sigma_{FM}^{\uparrow}}\right)\frac{1}{2\lambda_{SC}}\right)$$

- The equation contains only materials parameters of ferromagnet and semiconductor and “experimental” variable – current
- it allows finding $c^{\uparrow}$

Heaving found $c^{\uparrow}$ we can obtain the values of all coefficients of solution of the problem. The coefficients* are (the exact form of expressions is taken verbatim from T. Schäpers [11])

$$c^{\uparrow}=-\frac{\lambda_{SC}}{\sigma_{SC}}\frac{e\,j\,\beta(1-\beta)}{1+\frac{\lambda_{SC}}{\lambda_{FM}}\frac{\sigma_{FM}}{\sigma_{SC}}(1-\beta)^2} \qquad c^{\downarrow}=+\frac{\lambda_{SC}}{\sigma_{SC}}\frac{e\,j\,\beta(1+\beta)}{1+\frac{\lambda_{SC}}{\lambda_{FM}}\frac{\sigma_{FM}}{\sigma_{SC}}(1-\beta)^2} \qquad \beta=\frac{D_{\uparrow}(E_F)-D_{\downarrow}(E_F)}{D_{\uparrow}(E_F)+D_{\downarrow}(E_F)}$$

$$d^{\uparrow}=-d^{\downarrow}=-\frac{\lambda_{SC}}{\sigma_{SC}}\frac{e\,j\,\beta}{1+\frac{\lambda_{SC}}{\lambda_{FM}}\frac{\sigma_{FM}}{\sigma_{SC}}(1-\beta)^2} \qquad \mu_{off}=+\frac{\lambda_{SC}}{\sigma_{SC}}\frac{e\,j\,\beta^2}{1+\frac{\lambda_{SC}}{\lambda_{FM}}\frac{\sigma_{FM}}{\sigma_{SC}}(1-\beta)^2} \qquad a=-\frac{e\,j}{\sigma_{FM}} \qquad b=-\frac{e\,j}{\sigma_{SC}}$$

Using these coefficients the electrochemical potential for both spin channels, both in ferromagnet and in semiconductor, can be calculated

*the equations are just for reference -do not try to memorize them

Using coefficients from previous slide we can plot the electrochemical potential in the ferromagnet and in the semiconductor

$$\mu^{\uparrow,\downarrow}(x)=\mu_0^{FM}+a\,x+c^{\uparrow,\downarrow}e^{x/\lambda_{FM}} \qquad \text{for } x\leq 0$$
$$\mu^{\uparrow,\downarrow}(x)=\mu_0^{SC}+b\,x+d^{\uparrow,\downarrow}e^{-x/\lambda_{SC}} \qquad \text{for } x>0$$

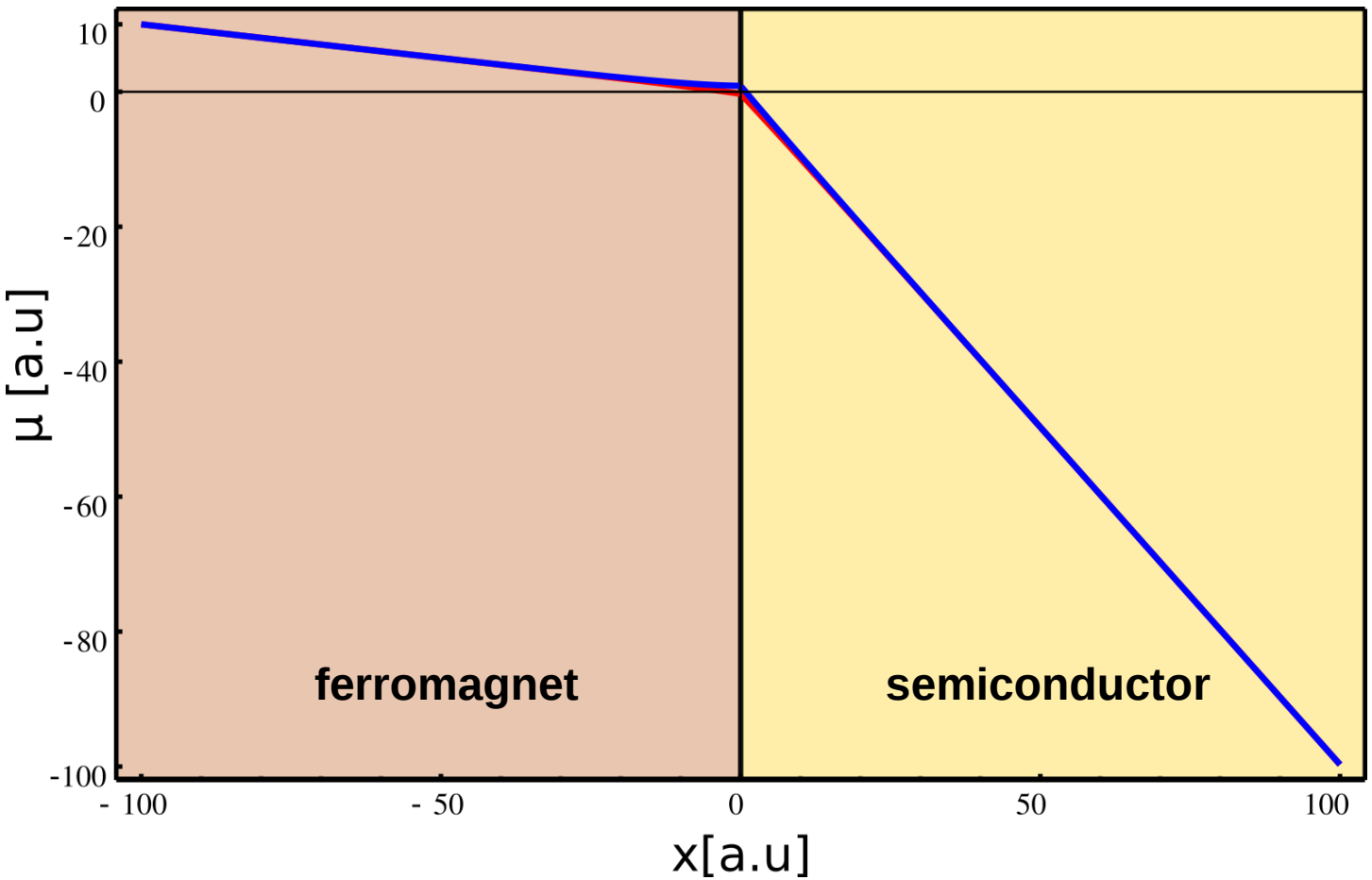

- Conductivity of the ferromagnet **10** times higher than that of the semiconductor
- The same spin-diffusion length both in the ferromagnet and in the semiconductor

$$\beta=0.5$$
$$\lambda_{SC}=10$$
$$\lambda_{FM}=10$$

$$\frac{\sigma_{FM}}{\sigma_{SC}}=10$$

- Not that different slopes of μ versus x in both regions reflects different conductivities

Mathematica 9 code to get the plot:

```
cup[e_,j_,B_,Lsc_,Lfm_,Ssc_,Sfm_]=-(Lsc/Ssc)*(e j B (1-B))/(1+Lsc/Lfm*Sfm/Ssc (1-B^2));
cdown[e_,j_,B_,Lsc_,Lfm_,Ssc_,Sfm_]=Lsc/Ssc*(e j B (1+B))/(1+Lsc/Lfm*Sfm/Ssc (1-B^2));
dup[e_,j_,B_,Lsc_,Lfm_,Ssc_,Sfm_]=-(Lsc/Ssc)*(e j B)/(1+Lsc/Lfm*Sfm/Ssc (1-B^2));
ddown[e_,j_,B_,Lsc_,Lfm_,Ssc_,Sfm_]=Lsc/Ssc*(e j B)/(1+Lsc/Lfm*Sfm/Ssc (1-B^2));
mu0[e_,j_,B_,Lsc_,Lfm_,Ssc_,Sfm_]=Lsc/Ssc*(e j B^2)/(1+Lsc/Lfm*Sfm/Ssc (1-B^2));
e=1;
j=1;
B=0.5;
Lsc=10;
Lfm=10;
Ssc=1;
Sfm=10;
(*FMup and SCup,FMdown and SCdown*)
Plot[{Piecewise[{{-((e j)/Sfm) x +cup[e,j,B,Lsc,Lfm,Ssc,Sfm]*Exp[x/Lfm],x<=0},{mu0[e,j,B,Lsc,Lfm,Ssc,Sfm]-((e j)/Ssc) x +dup[e,j,B,Lsc,Lfm,Ssc,Sfm]*Exp[-x/Lfm],x>0}}],Piecewise[{{-((e j)/Sfm) x +cdown[e,j,B,Lsc,Lfm,Ssc,Sfm]*Exp[x/Lfm],x<=0},{mu0[e,j,B,Lsc,Lfm,Ssc,Sfm]-((e j)/Ssc) x
+ddown[e,j,B,Lsc,Lfm,Ssc,Sfm]*Exp[-x/Lfm],x>0}}]},{x,-100,100}, Frame->True,PlotStyle->{{RGBColor[1,0,0], Thickness[0.005]},{RGBColor[0,0,1],Thickness[0.005]},{RGBColor[0,0,1],Thickness[0.002]},{RGBColor[1,0.5,0.5],Thickness[0.002]}},AxesStyle->Directive[GrayLevel[0],AbsoluteThickness[1]],ImageSize-
>{600},BaseStyle->{FontSize->20, FontWeight->"Normal"},FrameStyle->Directive[AbsoluteThickness[2]],FrameTicks->{{Union[Table[-100+i*20,{i,0,5}],{10}],None},{Automatic,None}}]
```

Using coefficients from previous slide we can plot the electrochemical potential in the ferromagnet and in the semiconductor

$$\mu^{\uparrow,\downarrow}(x)=\mu_0^{FM}+a\,x+c^{\uparrow,\downarrow}e^{x/\lambda_{FM}} \qquad \text{for } x\leq 0$$
$$\mu^{\uparrow,\downarrow}(x)=\mu_0^{SC}+b\,x+d^{\uparrow,\downarrow}e^{-x/\lambda_{SC}} \qquad \text{for } x>0$$

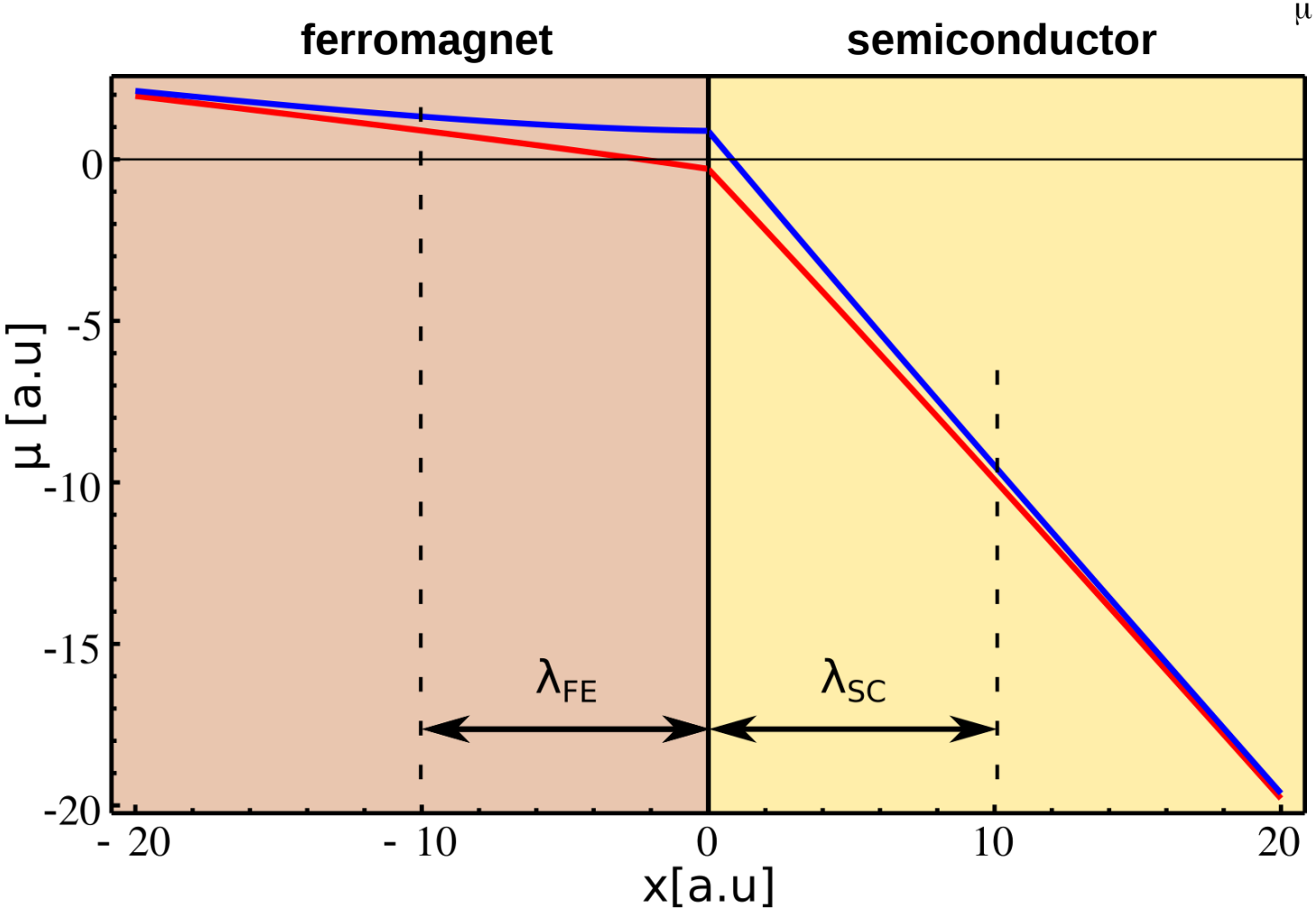

- Conductivity of the ferromagnet **10** times higher than that of the semiconductor
- The same spin-diffusion length both in the ferromagnet and in the semiconductor

$$\beta=0.5$$
$$\lambda_{SC}=10$$
$$\lambda_{FM}=10$$

$$\frac{\sigma_{FM}}{\sigma_{SC}}=10$$

- Not that different slopes of μ versus x in both regions reflects different conductivities

- electrons from **up** and **down** spin channels have different electrochemical potential roughly within spin diffusion length from the ferromagnet/semiconductor interface.
- within the bulk of the semiconductor the potentials are equal.

Using coefficients from previous slide we can plot the electrochemical potential in the ferromagnet and in the semiconductor

$$\mu^{\uparrow,\downarrow}(x)=\mu_0^{FM}+a\,x+c^{\uparrow,\downarrow}e^{x/\lambda_{FM}} \qquad \text{for } x\leq 0$$
$$\mu^{\uparrow,\downarrow}(x)=\mu_0^{SC}+b\,x+d^{\uparrow,\downarrow}e^{-x/\lambda_{SC}} \qquad \text{for } x>0$$

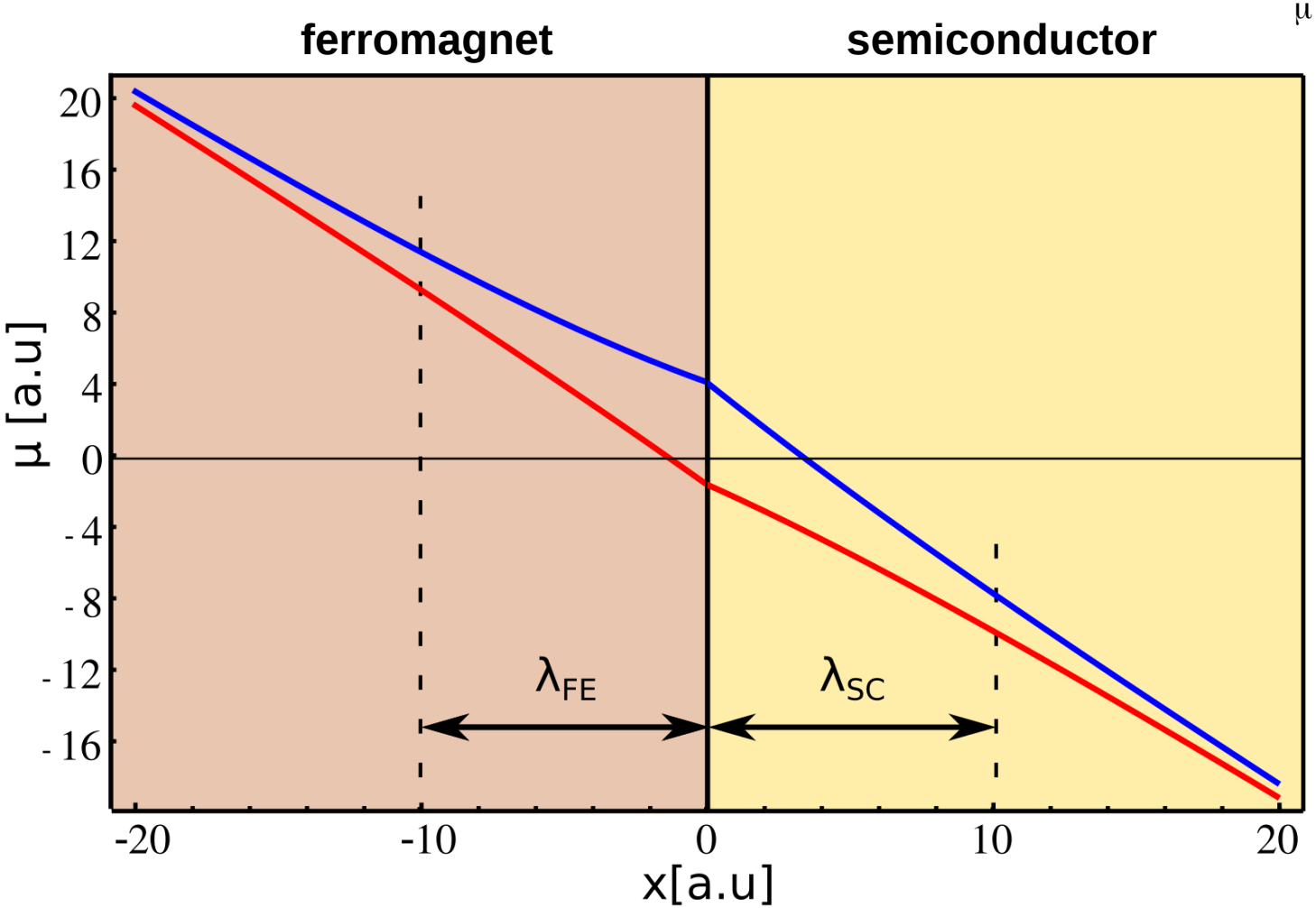

- Conductivity of the ferromagnet equal to that of the semiconductor
- The same spin-diffusion length both in the ferromagnet and in the semiconductor

$$\beta=0.5$$
$$\lambda_{SC}=10$$
$$\lambda_{FM}=10$$

$$\frac{\sigma_{FM}}{\sigma_{SC}}=1$$

- Lower conductivity mismatch results in higher difference between $\mu^{\uparrow}$ and $\mu^{\downarrow}$ at the interface

Knowing electrochemical potential and the conductivities (different for both spin channels) we can calculate the currents (the expression here is for a ferromagnet)

$$j^{\uparrow,\downarrow}=-\frac{\sigma_{FM}^{\uparrow,\downarrow}}{e}\frac{\partial\mu^{\uparrow,\downarrow}}{\partial x}=-\frac{\sigma_{FM}^{\uparrow,\downarrow}}{e}\left(a+\frac{c^{\uparrow,\downarrow}}{\lambda_{FM}}e^{x/\lambda_{FM}}\right)$$

note that coefficient c depends only on the total conductivity of ferromagnet and not on channel conductivities ($\sigma^{\uparrow}$ and $\sigma^{\downarrow}$)

$$\beta=\frac{\sigma_{FM}^{\uparrow}-\sigma_{FM}^{\downarrow}}{\sigma_{FM}^{\uparrow}+\sigma_{FM}^{\downarrow}}$$

$$+$$

$$\sigma_{FM}^{\uparrow}+\sigma_{FM}^{\downarrow}=\sigma_{FM}$$

$$\sigma_{FM}^{\uparrow}=\frac{1}{2}\sigma_{FM}(1+\beta)$$

$$\sigma_{FM}^{\downarrow}=\frac{1}{2}\sigma_{FM}(1-\beta)$$

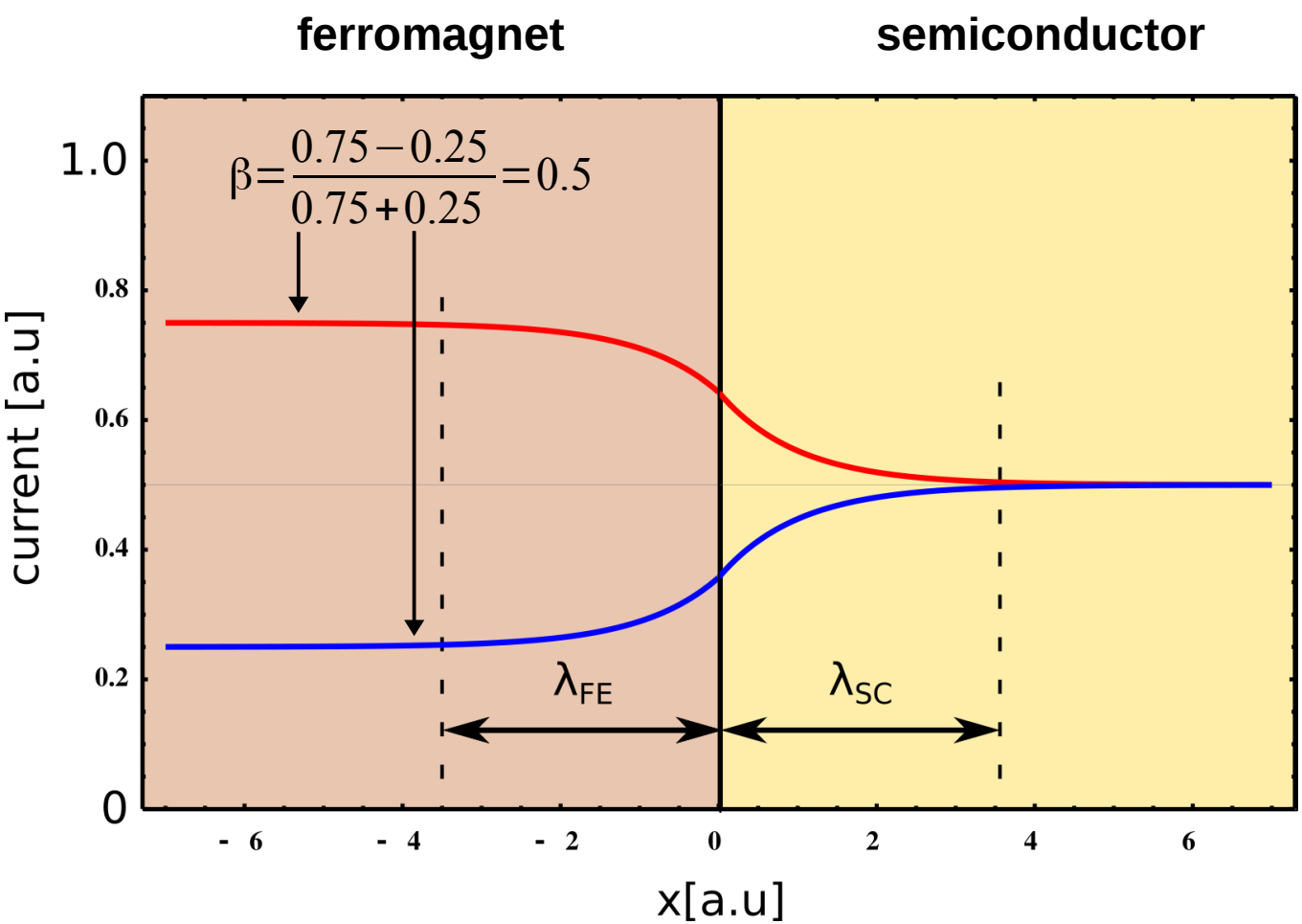

$\beta=0.5$

- Note that due to the diffusion the spin asymmetry is different from bulk values on both sides of the interface

Knowing electrochemical potential and the conductivities (different for both spin channels) we can calculate the currents (the expression here is for a ferromagnet)

$$j^{\uparrow,\downarrow} = -\frac{\sigma_{FM}^{\uparrow,\downarrow}}{e}\frac{\partial \mu^{\uparrow,\downarrow}}{\partial x} = -\frac{\sigma_{FM}^{\uparrow,\downarrow}}{e}\left(a + \frac{c^{\uparrow,\downarrow}}{\lambda_{FM}} e^{x/\lambda_{FM}}\right)$$

note that coefficient c depends only on the total conductivity of ferromagnet and not on channel conductivities ($\sigma^{\uparrow}$ and $\sigma^{\downarrow}$)

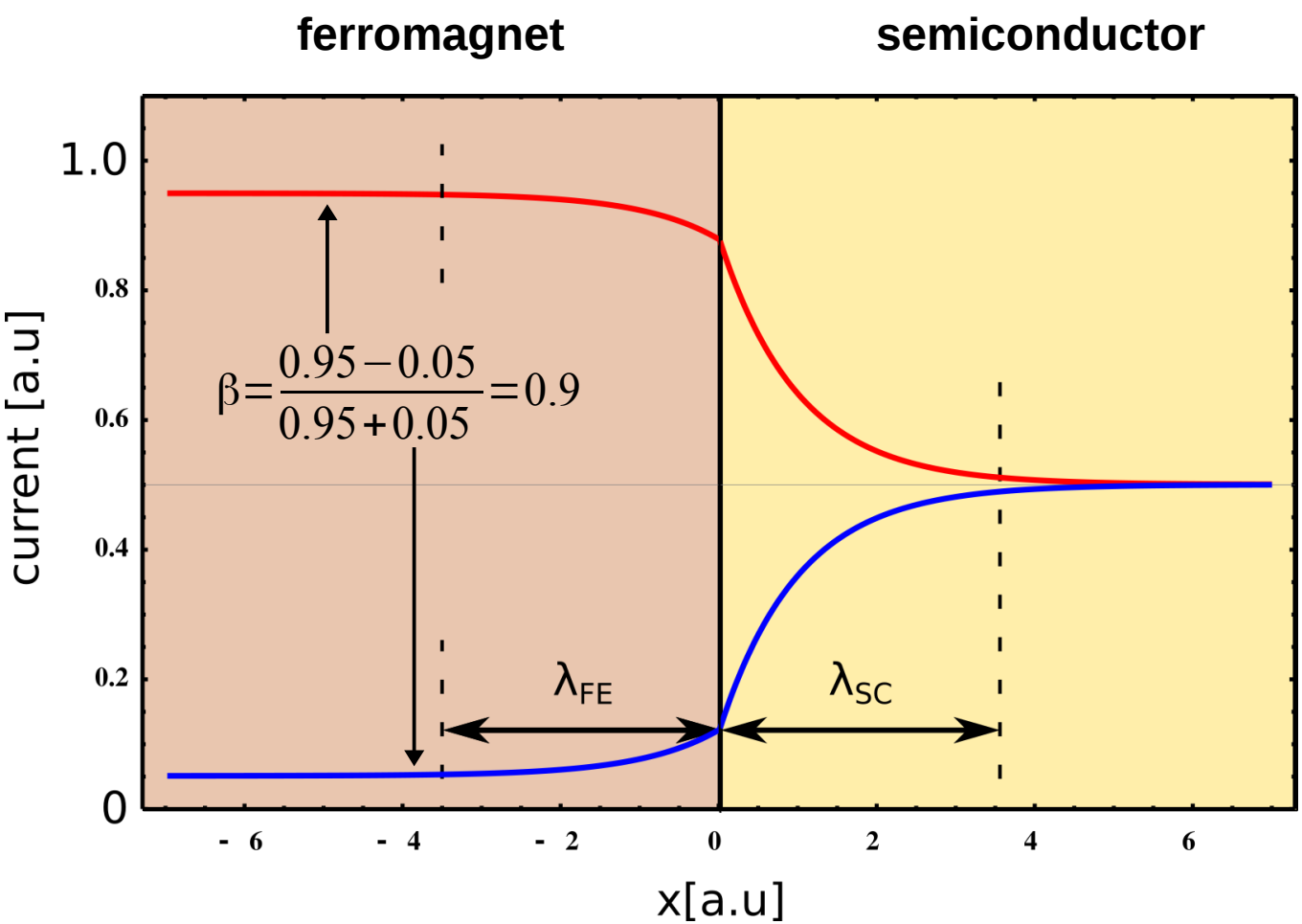

β=0.9

- Note that due to the diffusion the spin asymmetry is different from bulk values on both sides of the interface

Transport regimes

The characteristic, material, length scales for electron transport are [11]:

- mean free path (both elastic* and inelastic)
- phase-coherence length – distance covered before the phase is randomized – scattering on phonons
- spin-diffusion length

Size of the sample ***L*** in relation to characteristic transport lengths determines the transport regime

Diffusive	Classical	$\lambda_F, l_\varphi, l_e \ll L$
	Quantum	$\lambda_F, l_e \ll L < l_\varphi$
Ballistic	Classical	$\lambda_F \ll L < l_\varphi, l_e$
	Quantum	$\lambda_F, L < l_e < l_\varphi$

λ_F-Ferrmi wavelength
l_ϕ-phas-coherence length
l_e-mean free path (mfp)

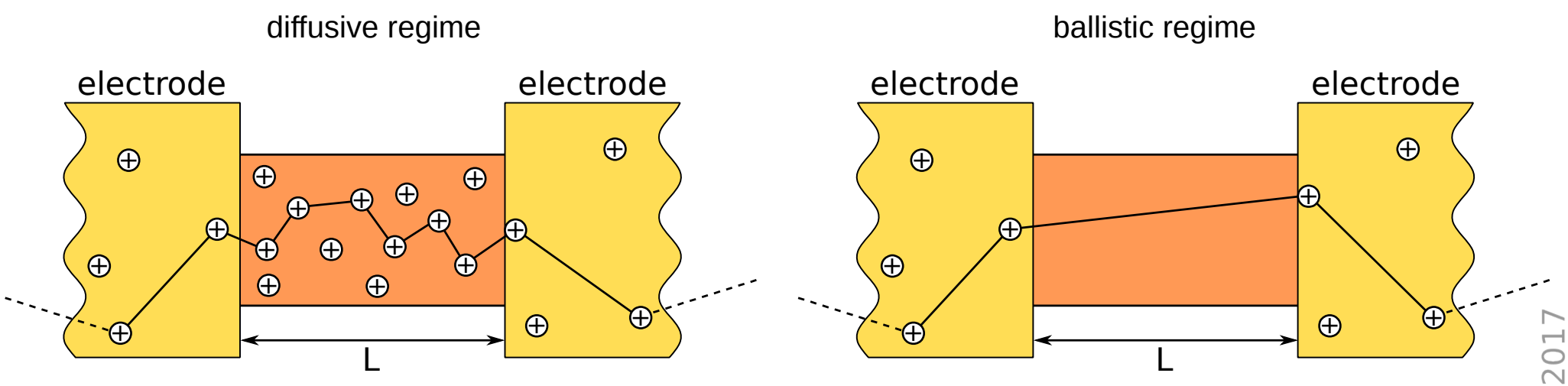

*no energy transfer, e.g., scattering on charged impurity

Transport regimes

The characteristic, material, length scales for electron transport are [11]:

- mean free path (both elastic* and inelastic)
- phase-coherence length – distance covered before the phase is randomized – scattering on phonons
- spin-diffusion length

Size of the sample ***L*** in relation to characteristic transport lengths determines the transport regime

Diffusive	Classical	$\lambda_F, l_\varphi, l_e \ll L$
	Quantum	$\lambda_F, l_e \ll L, l_\varphi$
Ballistic	Classical	$\lambda_F \ll L < l_\varphi, l_e$
	Quantum	$\lambda_F, L < l_e < l_\varphi$

λ_F-Ferrmi wavelength
l_ϕ-phas-coherence length
l_e-mean free path (mfp)

- in the **quantum limit** the phase coherence length exceeds the elastic mean free path

$$l_e < l_\phi$$

Predictable phase of wave function and predictable change of phase on scattering

classical regime

quantum regime

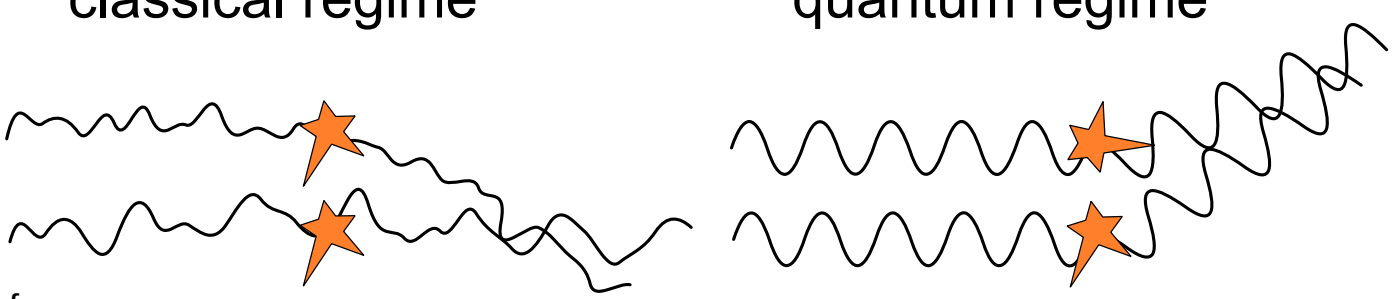

Phase of wave function and change of phase on scattering not predictable

*no energy transfer, e.g., scattering on charged impurity

Two dimensional electron gas (2DEG)

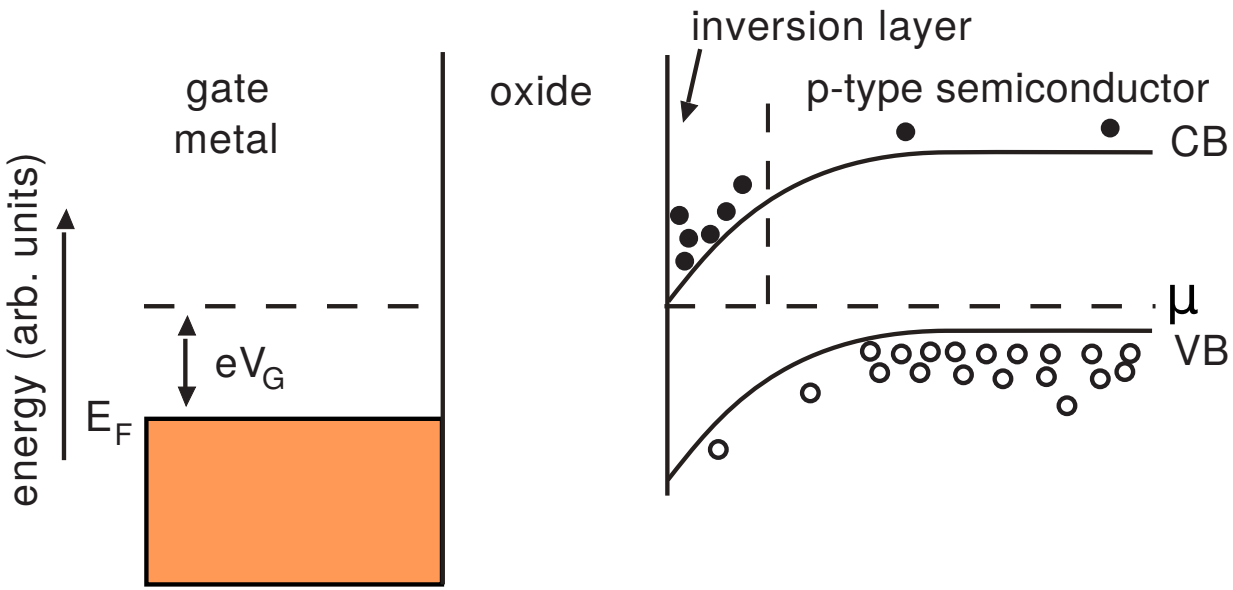

- the negative voltage applied to a metal gate induces n-type region in its vicinity (inversion layer) that is rich in electron carriers
- in MOSFET transistors this creates a conducting channel between n-type source and drain

"***magnetoelectric effects are precluded from bulk ferromagnetic*** *metals due to the very short screening length, in films thinner than a few nanometers, spin-dependent charge screening and band level shifting can lead to pronounced electric field-driven changes to magnetic properties.*" [23]

image from http://users-phys.au.dk/philip/pictures/physicsfigures/physicsfigures.html

InGaAs/InPt heterostructure - two dimensional electron gas (2DEG)

image from Th. Schäpers, J. Knobbe, van der Hart, and H. Hardtdegen, Science and Technology of Advanced Materials **4**, 19 (2003)

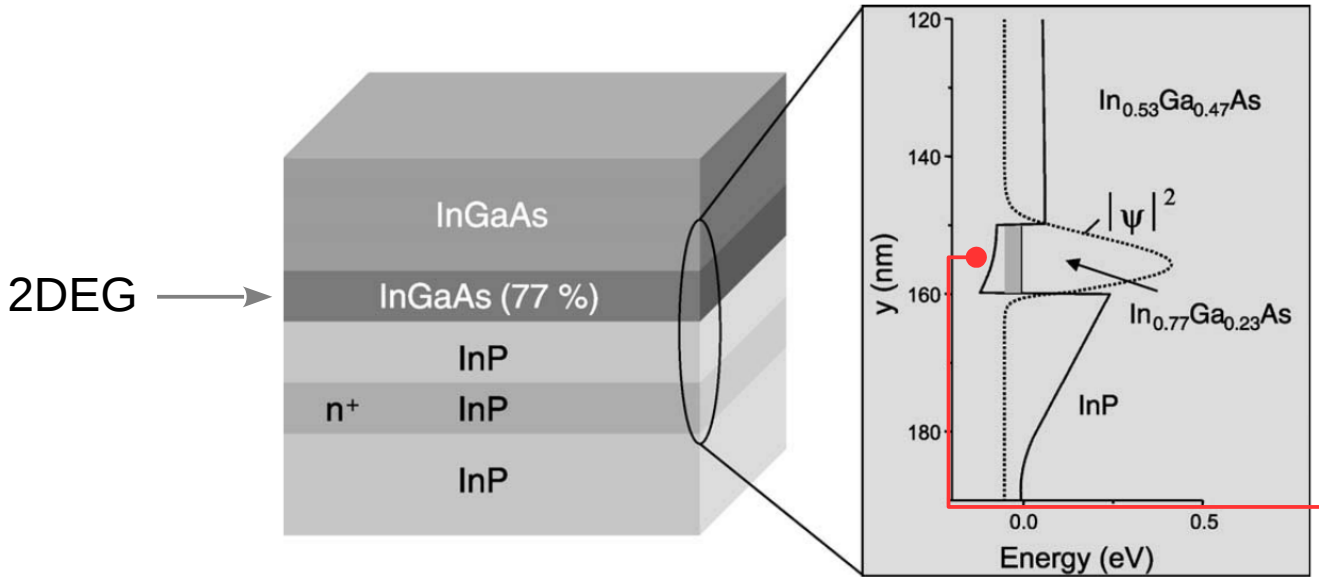

Fig. 2. Schematic illustration of the layer sequence of the InGaAs/InP heterostructure. The right panel shows the conduction band profile and the probability amplitude $|\Psi|^2$ of the envelope function.

- InP – semi-insulating, high carrier mobility
- InP lattice constant match $In_{0.53}Ga_{0.47}As$ at RT [15]
- $In_{0.77}Ga_{0.23}As$ layer is strained due to lattice mismatch

- the electron wave function is located mainly in the strained $In_{0.53}Ga_{0.47}As$ layer
- the electrons in the 2DEG layer come from negatively doped InP layer [11]
- the tilted potential profile results in an electric field in the quantum well [11]
- high mobilities in 2DEG ≈10^5 cm^2/Vs [(cm/s)/V] at 40K

The Rashba effect

- the electric field in 2DEG is oriented perpendicularly to its plane
- electrons moving from the source to the drain experience the effective magnetic field given by Lorentz transformation [16]:

$$B'_{\parallel} = B \qquad B'_{\perp} = \frac{(\vec{B} - (\vec{v}/c^2)) \times \vec{E}\perp}{\sqrt{(1 - v^2/c^2)}} \rightarrow B'_{\perp} = \frac{(\vec{v}/c^2) \times \vec{E}}{\sqrt{(1 - v^2/c^2)}}$$

we assume that there is no external magnetic field

- the magnetic field experienced by the electrons is oriented perpendicularly ($\vec{v} \times \vec{E}$) to the plane described by their velocity and the electric field

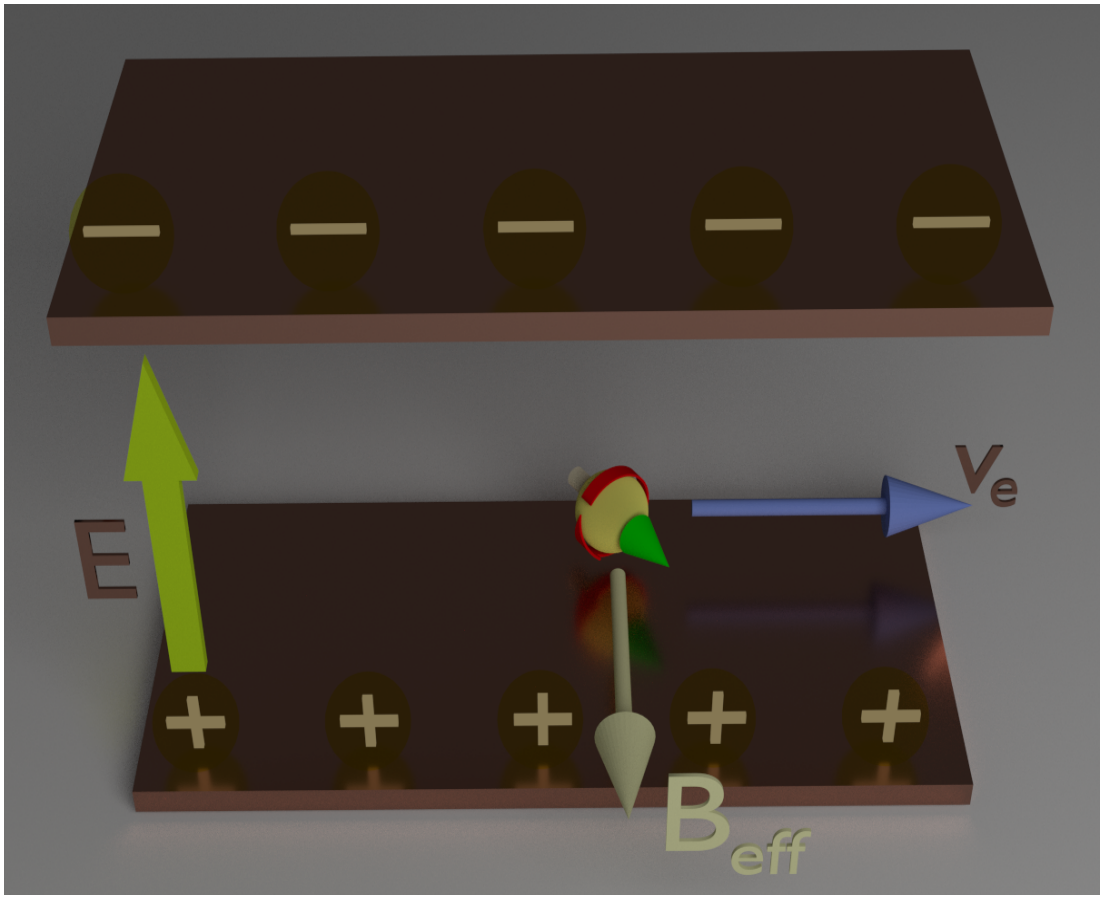

- charged plates are the source of a magnetic field experienced by moving electrons
- the electrons/spins precess in the magnetic field

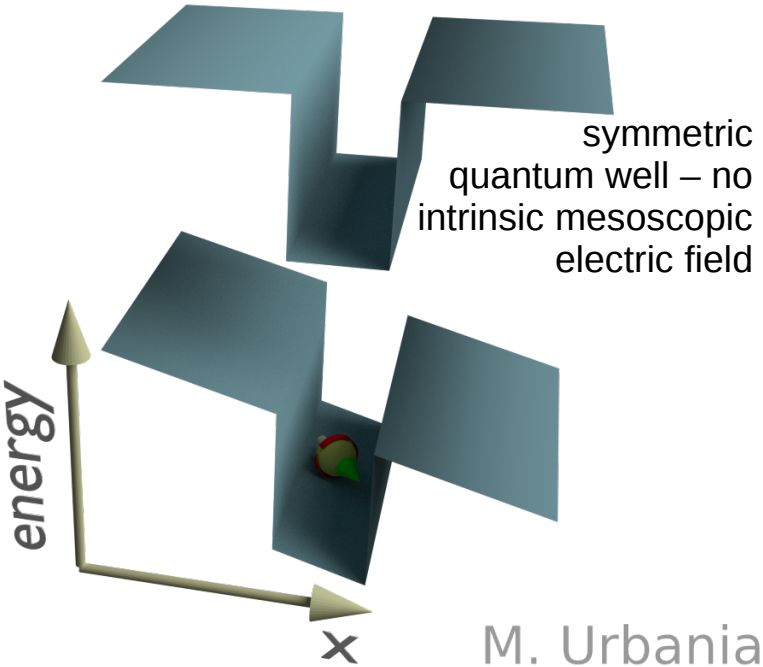

symmetric quantum well – no intrinsic mesoscopic electric field

The Rashba effect

- the electric field in 2DEG is oriented perpendicularly to its plane
- electrons moving from the source to the drain experience the effective magnetic field given by Lorentz transformation [16]:

$$B'_{\parallel} = B \qquad B'_{\perp} = \frac{(\vec{B} - (\vec{v}/c^2)) \times \vec{E}\perp}{\sqrt{(1 - v^2/c^2)}} \rightarrow B'_{\perp} = \frac{(\vec{v}/c^2) \times \vec{E}}{\sqrt{(1 - v^2/c^2)}}$$

we assume that there is no external magnetic field

- the magnetic field experienced by the electrons is oriented perpendicularly ($\vec{v} \times \vec{E}$) to the plane described by their velocity and the electric field

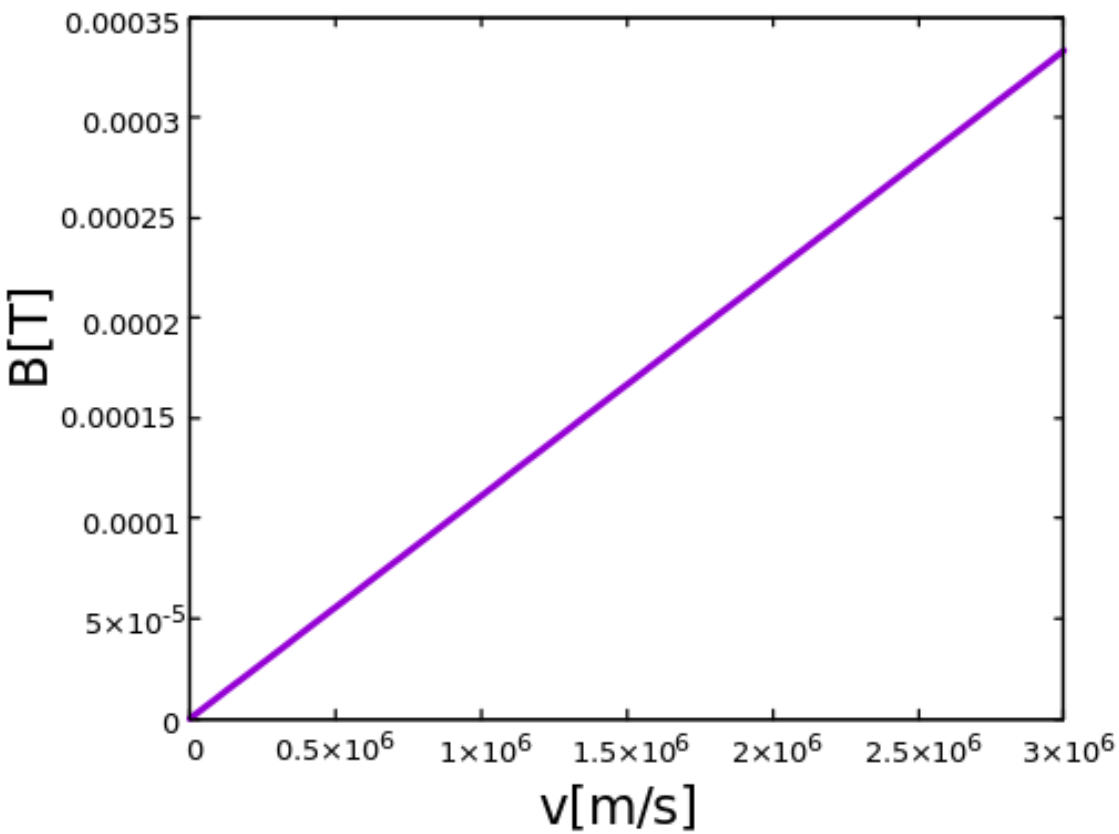

E=10^7 V/m

- in III-V semiconductor structures additional contribution to spin-orbit interaction comes from **Dresselhaus effect** caused by bulk inversion asymmetry [19]

- high mobilities in 2DEG ≈10^5 cm^2/Vs [(cm/s)/(V/cm)] (10 m^2/Vs) at 40K

The Rashba effect

- the effect is analogous to spin orbit coupling responsible for the magnetocrystalline anisotropy (there the electric field is due to the charge of the nucleus)

The Hamiltonian of the interaction can be written as [11]:

$$\hat{H}_{Rashba} = \alpha_R \hat{z} \left(\vec{\sigma} \times \vec{k}\right),$$

$\vec{k} = \vec{p}/\hbar$ -wave vector of the electron

α_R - Rashba parameter - strength of the coupling

The Rashba parameter depends not only on the mesoscopic electric field acting on electrons in 2DEG but also on *the potential gradients due to electron orbitals of the atoms forming the crystal* [11$_{p.153}$, 19].
The greater atomic number the higher α_R.(example indium or antimony).

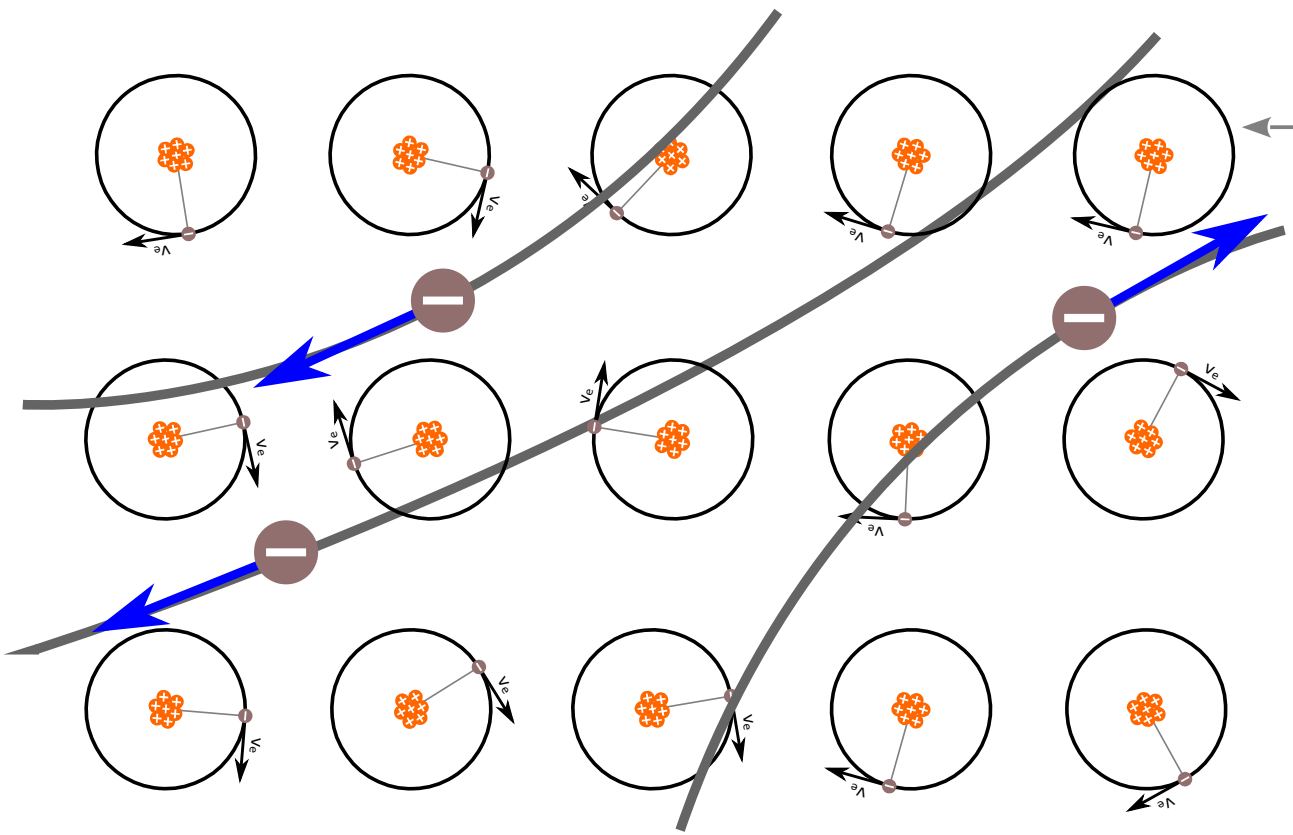

external “Rashba field” is superimposed on local fields of ions

The Rashba effect

The energy splitting of the electrons in the Rashba magnetic field is [11]:

$$E_R = \pm \alpha_R |\vec{k}|$$

For fixed energy (here Fermi energy) the wave vector difference is given by [11]:

$$\Delta k_R = \frac{2 m^* \alpha_R}{\hbar^2}$$

constant effective mass m^* assumed

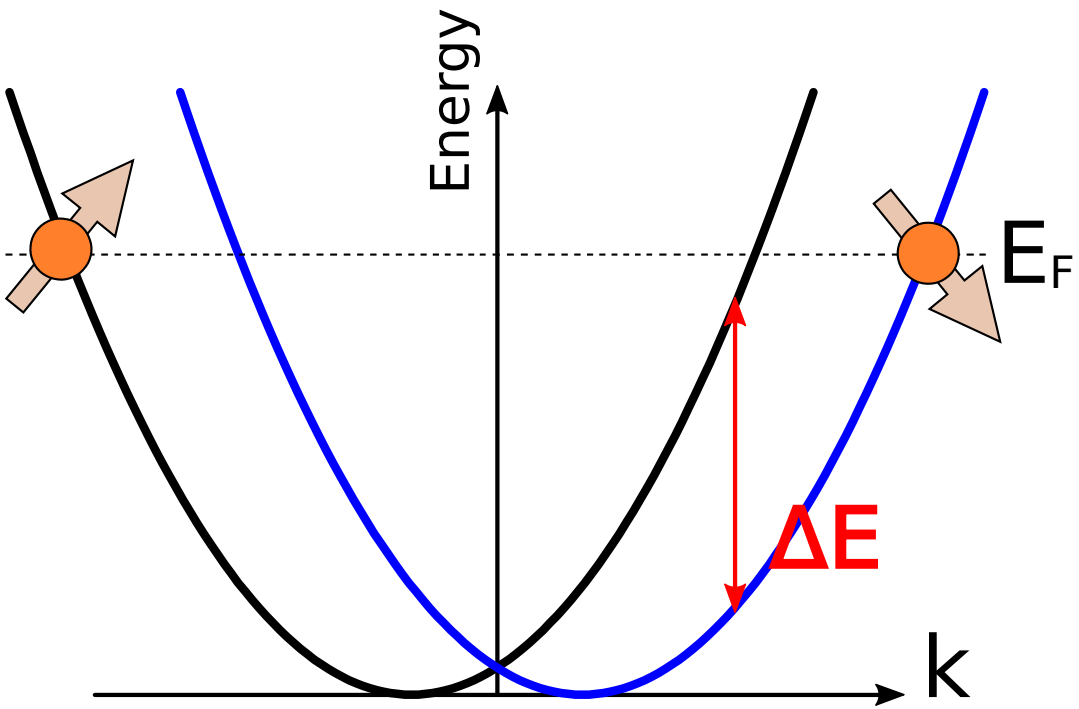

image adapted from Fig. 7.4 of T. Schäpers *Semiconductor Spintronics*, De Gruyter 2016 [11]

Gate control of the spin-orbit interaction

- MBE grown structures
- the gate electrode was made on the top of the 100-nm-thick SiO_2 insulating layer which covers the hall bar

2DEG

ud-$In_{0.52}Al_{0.48}As$ gate Schottky layer (20 nm)
ud-$In_{0.53}Ga_{0.47}As$ channel layer (20 nm)
ud-$In_{0.52}Al_{0.48}As$ spacer layer (6 nm)
n^+-$In_{0.52}Al_{0.48}As$ carrier-supply layer (7 nm , n=4 x 10^{18} cm^{-3})
ud-$In_{0.52}Al_{0.48}As$ buffer layer
S. I.-InP substrate

FIG. 1. Schematic layer structure of an inverted $In_{0.53}Ga_{0.47}As/In_{0.52}Al_{0.48}As$ heterostructure.

α_R can be controlled by gate voltage

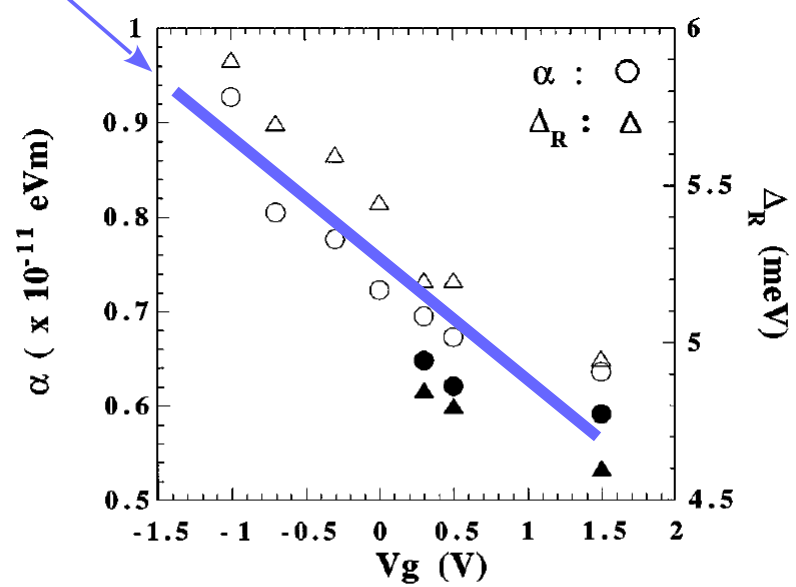

FIG. 5. Gate voltage dependence of the spin-splitting energies Δ_R and the spin-orbit interaction constant α. Circles are the spin-orbit interaction parameters, and triangles are the spin-splitting energy. The open circles and triangles were obtained by fitting the first node positions. The filled symbols were obtained by fitting the second node positions.

"We have experimentally demonstrated that α can be controlled by the interface electric field **because the Rashba mechanism is dominant**. This result suggests that the precession of the injected polarized spin can be controlled by the gate voltage. **This is the first step for realizing the spin-polarized field effect transistor**."

images from J. Nitta, T. Akazaki, H. Takayanagi, and T. Enoki, Phys.Rev.Lett. **78**, 1335 (1997) [17]

Gate control of the spin-orbit interaction – switching off the coupling?

Asymmetric quantum well (QW) (eg. $Ga_{0.47}In_{0.53}As$ (well), $Al_{0.48}In_{0.52}As$ (left barrier), and $Al_xGa_{1-x}As_ySb_{1-y}$ (right barrier))

$$|x - x_{optimum}| < 0.01:$$

$$E_z < 0 : \alpha_R \approx 0$$

$$E_z > 0 : \alpha_R \gg 1$$

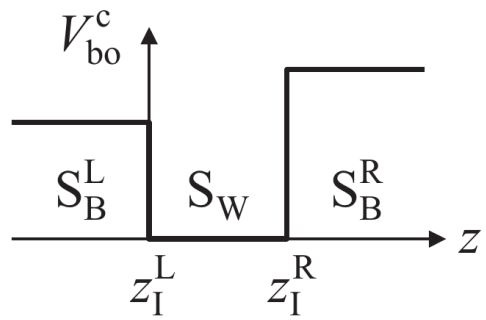

FIG. 1. A quantum-well structure consisting of three different semiconductors with the zinc-blende structure, S_B^L, S_W, and S_B^R. $V_{bo}^c(z)$ is the potential due to the conduction-band offset.

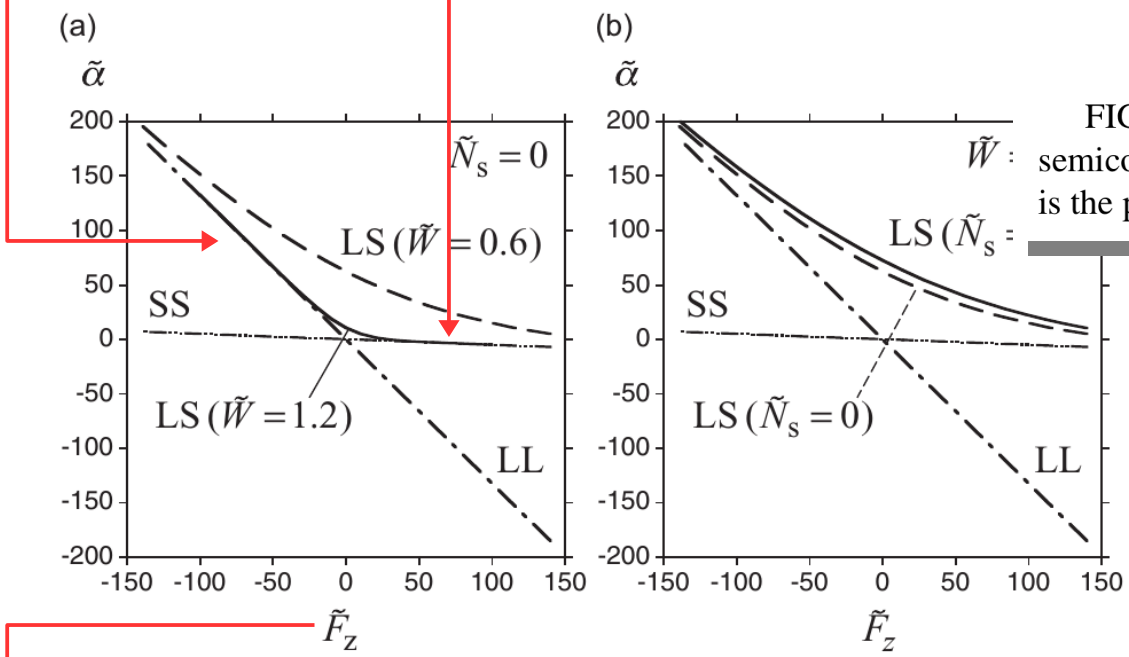

FIG. 4. Rashba coefficient α as a function of the external force $F_z = -eE_z^{ex}$ for three combinations of interfaces: LL, SS, and LS (see text). (a) The well-width (W) dependence for LS. (b) The electron-sheet-density (N_s) dependence for LS. The dimensionless Rashba coefficient is defined by $\tilde{\alpha} = (\alpha/\eta)/(\mathrm{Ry}^*/a_B^*)$. For the definition of other quantities, see the caption of Fig. 3.

- **the Rashba coefficient** α, which depends on the band offset, **can be tuned to be zero** by adjusting the Al fraction in the right barrier
- the α coefficient in composition adjusted asymmetric QW can be switched on by changing the polarity of the external field (theory!)
- required field > 10^7 V/m for 20nm thick QW → **0.2 V**

images from H. Akera, H. Suzuura, and Y. Egami, Phys. Rev. B **95**, 045301 (2017) [18]

- "*In a diffusive 2DEG, the momentum direction of electron changes frequently, and hence so does the direction of B_{eff}***" [19 p18]
- if δφ is the typical spin precession angle between the scattering events and there was N uncorrelated steps then the standard deviation of the precession angle is given by:

$$\sigma(\phi)=\delta\phi\sqrt{N} \qquad N=\frac{t}{\tau}$$

- spin relaxation time τ_s is a time after which the standard deviation becomes 1 - the time scale on which spin loses its memory

There are several basic mechanisms responsible for spin relaxation in semiconductors:

- **Elliott–Yafet (EY)**
- **D'yakonov–Perel' (DP)**
- Bir–Aronov–Pikus (BAP)
- hyperfine interaction

Elliott–Yafet (EY) - a spin relaxation process caused by scattering via phonons, impurities, boundaries and so on.

- in semiconductors, the spin-up and spin-down states are **mixed by the spin-orbit interaction** of the constituent elements of the host material
- the spin state contains a small component of the opposite spin
- spin polarized electrons can thus flip after each scattering events although the probability of the spin flip might not be so high

** the Rashba magnetic field

D'yakonov–Perel' (DP) - a spin relaxation process caused by precession in the magnetic field that is due to spin-orbit coupling**

- in compound semiconductors without a center of inversion symmetry
- the spin degeneracy is lifted by the spin-orbit interaction
- precession starts again after each scattering in a randomly changed field**
- spin relaxation rate is proportional to the momentum relaxation time

$$\hat{H}_{Rashba} = \alpha_R \hat{z}\,(\vec{\sigma} \times \vec{k}),$$

$\vec{k} = \vec{p}/\hbar$ -wave vector of the electron

α_R - Rashba parameter - strength of the coupling

$$\frac{1}{\tau_{spin}} \propto \tau_{momentum}$$

-,i.e., the shorter the momentum relaxation time is, the lower the spin relaxation rate is

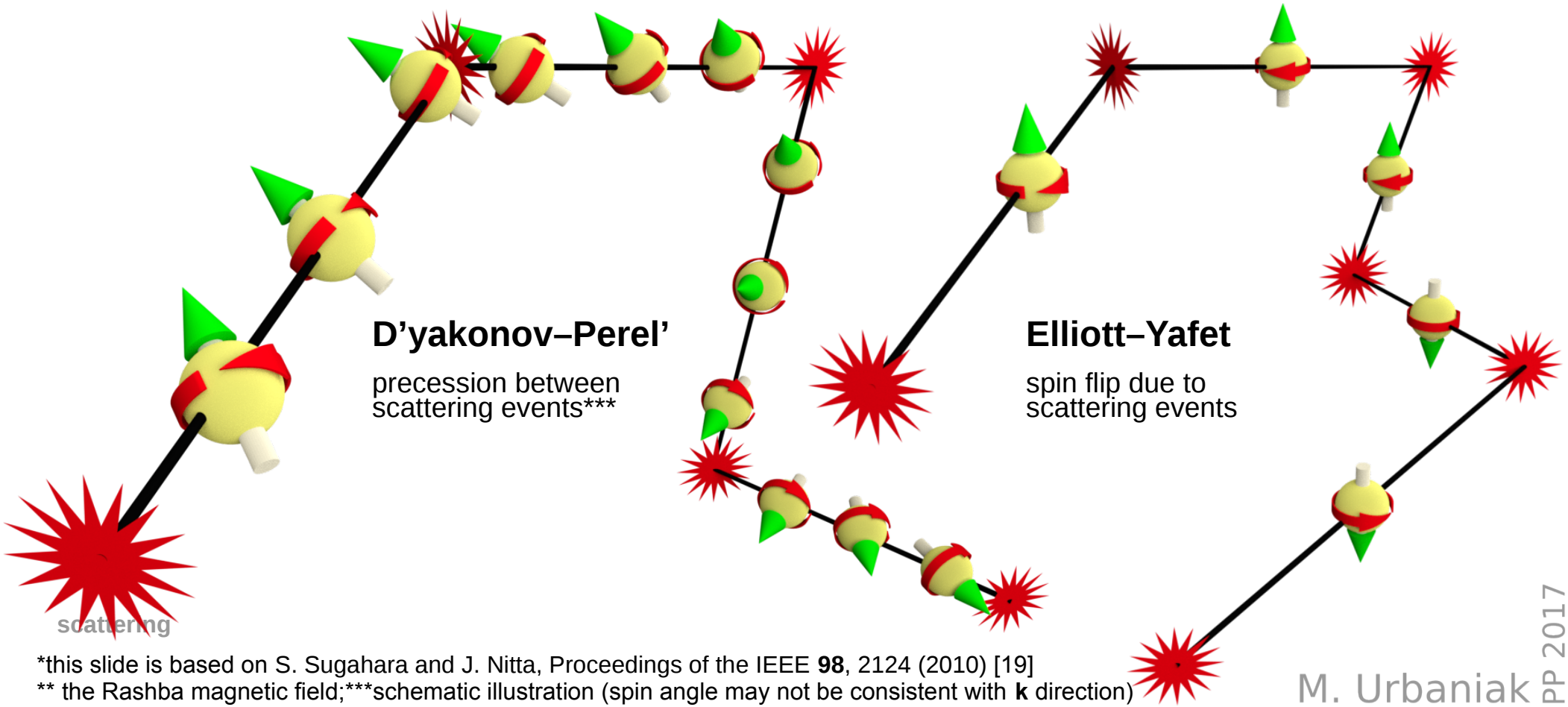

*this slide is based on S. Sugahara and J. Nitta, Proceedings of the IEEE **98**, 2124 (2010) [19]

** the Rashba magnetic field;***schematic illustration (spin angle may not be consistent with **k** direction)

Spin control with Rashba effect*

- spin orbit coupling is negligible for non-relativistic particles in vacuum but in semiconductors the spin-orbit interactions is enhanced by about **six orders** [19]

Spin FET – the key idea is that the spin orientation can be controlled by gate voltage instead of the external magnetic field

- because of the spin relaxation the electron loses its spin memory after certain number of scattering events

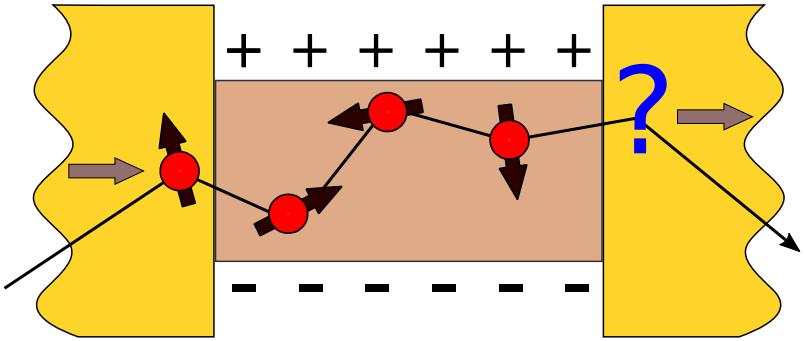

In spite of the **known** orientation of the spin entering the channel the orientation of the spin leaving the channel is **not known**

- if the transport through the channel is ballistic the Rashba effect can be used for deterministic control of the spin precession

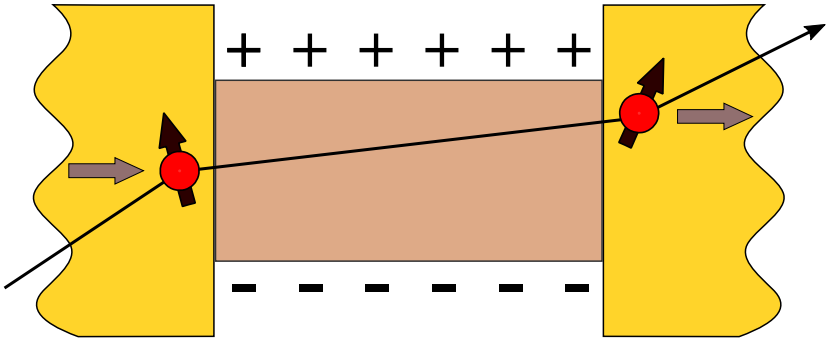

known orientation of the spin entering the channel and the **known** orientation of the spin leaving the channel

For diffusive (and ballistic) transport the so called **persistent spin helix** (PSH) [11,19] can be used **to suppress DP relaxation**.
PSH: the Rashba spin-orbit interaction strength α is equal to linear Dresselhaus spin-orbit interaction β [19]

- "*In this PSH condition, spin polarization is conserved even after scattering events*" [19]

- in PSH condition the effective spin-orbit coupling magnetic field is independent of electron's momentum and is directed along (x,-y,0) direction
- the spin precession angle in PSH condition is given by [19]:

$$\Delta\phi = \frac{2\alpha m^*}{\hbar^2} L \qquad L\text{ - channel length}$$

persistent spin helix condition*:

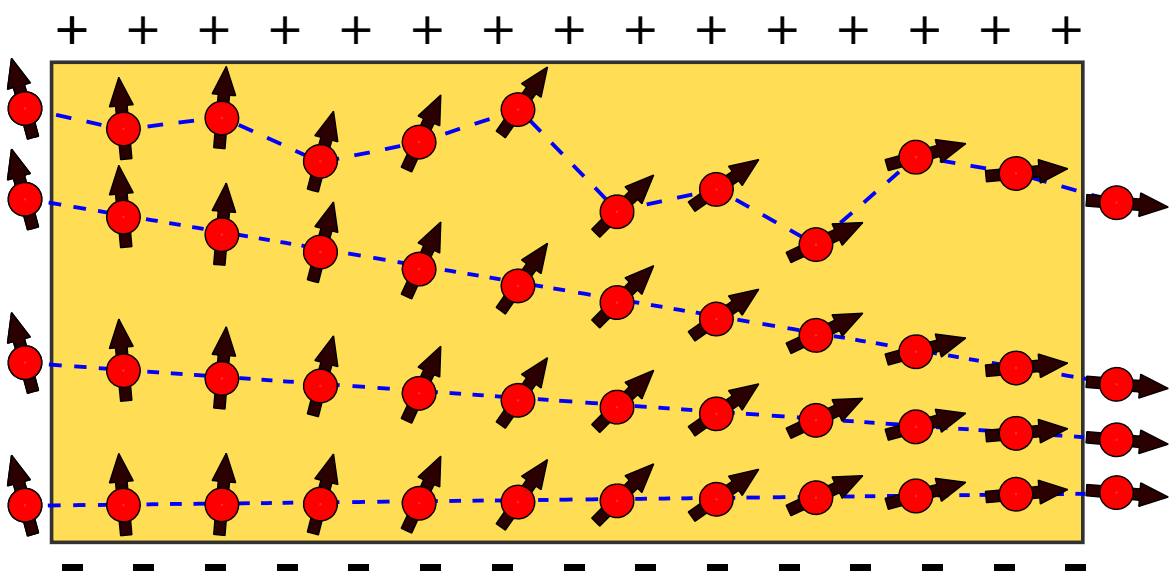

known orientation of the spin entering the channel and the **known** orientation of the spin leaving the channel independent of the path of the electron

*"This conservation is predicted to be robust against all forms of spin-independent scattering, including electron-electron interaction, but is broken by spin-dependent scattering and cubic Dresselhaus term" [19]

Datta and Das FET spin transistor

- change of the spin precession angle can be used to match the spin orientation of the electrons leaving the “Rashba channel” to the magnetization direction of the drain electrode

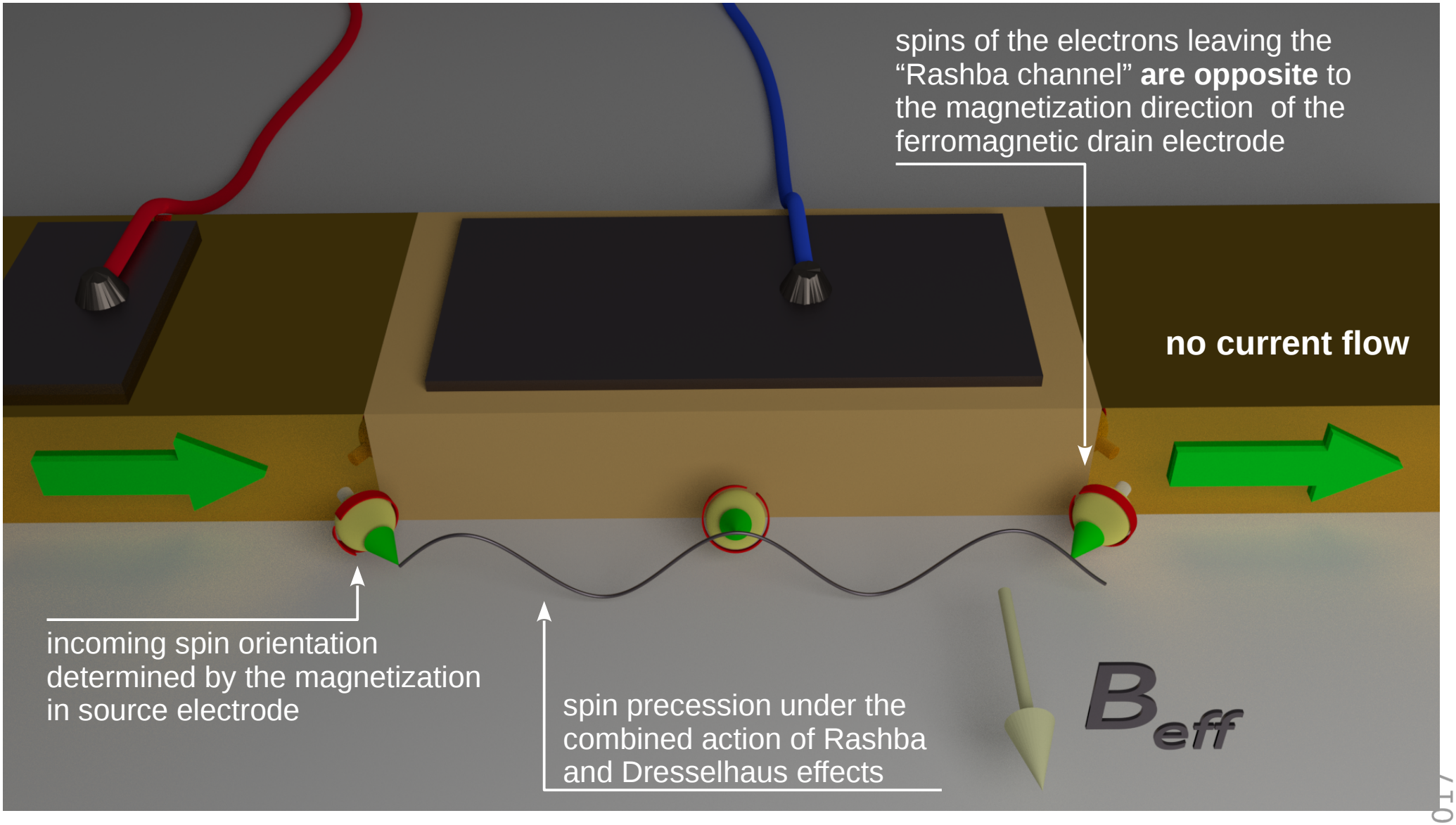

image based on Fig. 7.1 of T. Schäpers *Semiconductor Spintronics*, De Gruyter 2016 [11]

Datta and Das FET spin transistor

- change of the spin precession angle can be used to match the spin orientation of the electrons leaving the “Rashba channel” to the magnetization direction of the drain electrode

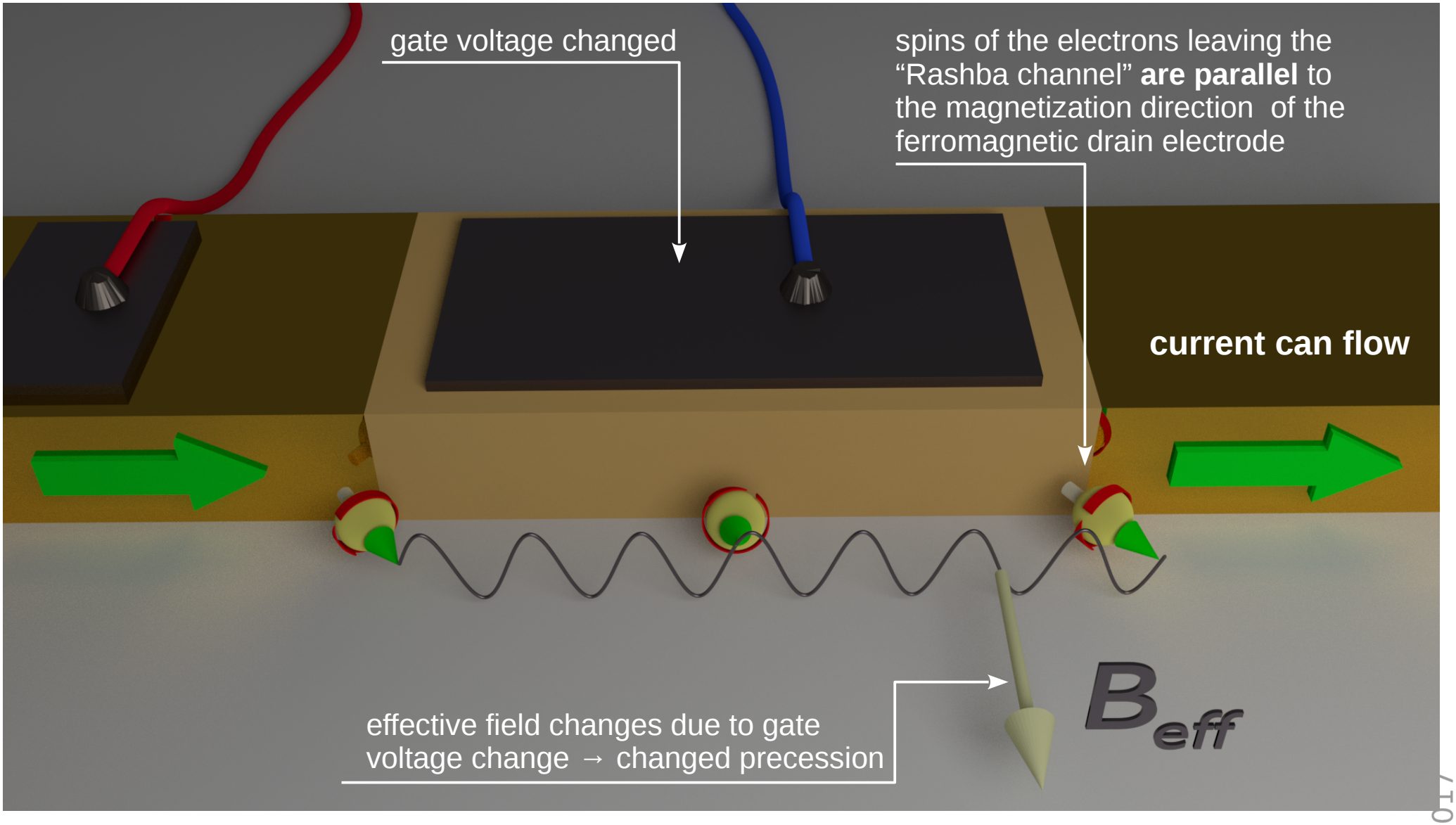

image based on Fig. 7.1 of T. Schäpers *Semiconductor Spintronics*, De Gruyter 2016 [11]

Voltage control of perpendicular magnetic anisotropy

- the perpendicular magnetic anisotropy controlled by the applied voltage
- voltage affects only the interface anisotropy of the CoFeB/oxide interface since the CoFeB film is thick enough in comparison with electrical screening length in metals [21]

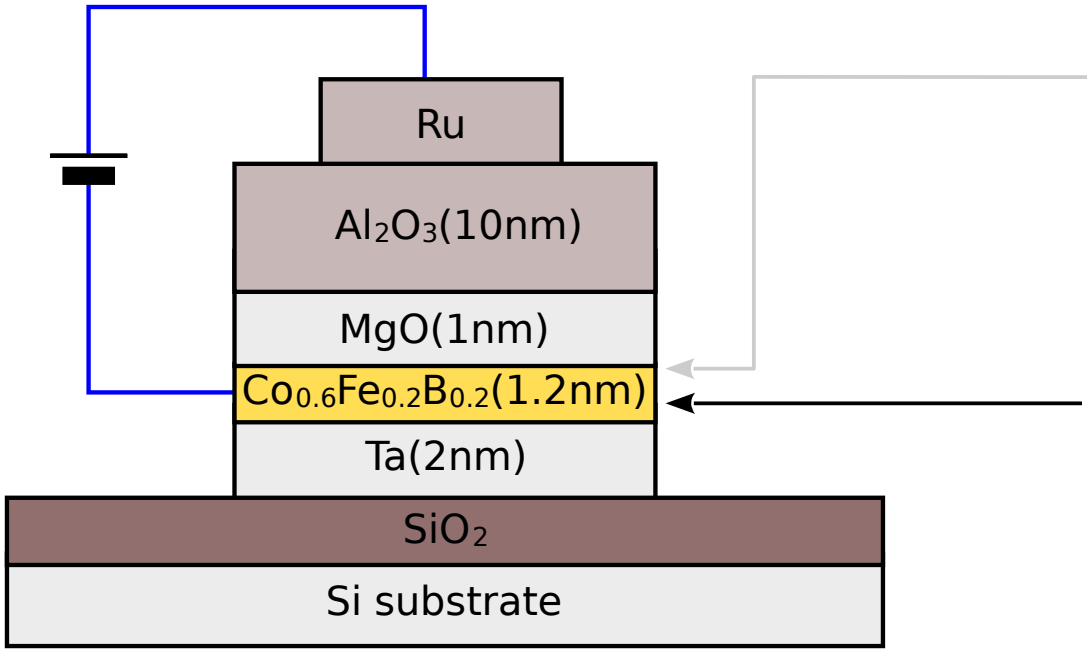

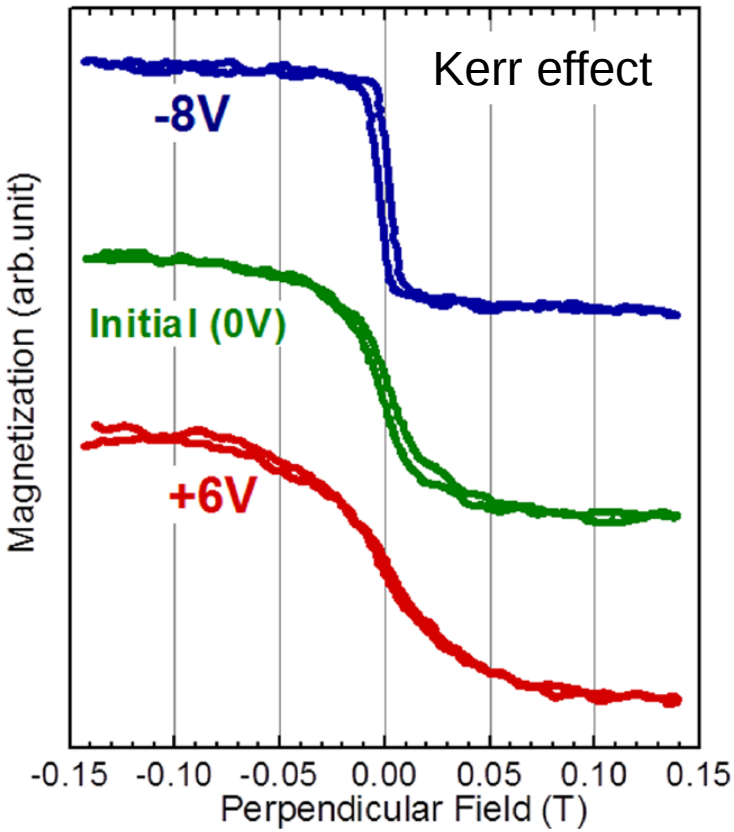

FIG. 3. Magnetization characteristics of $Co_{0.6}Fe_{0.2}B_{0.2}/MgO/Al_2O_3$ stack with $t_{CoFeB} = 12$A in a perpendicular magnetic field, observed by polar Kerr measurements. The voltage biases −8 V, 0 V, and +6 V were applied on the top Ru electrode, with the $Co_{0.6}Fe_{0.2}B_{0.2}$ layer grounded.

- the application of negative (**-8V**) voltage to Ru induces perpendicular magnetic anisotropy of CoFeB
- the negative bias decreases electron density at interfaces

graph from Koji Kita , D. W. Abraham, M.J. Gajek, and D.C. Worledge, J. Appl. Phys. **112**, 033919 (2012)

Spin transistor by anisotropy control - **concept**

- three terminal device with magnetic tunnel junction (MTJ)
- buffer layers/CrB(2.5nm)/thick-MgO*/CoFeB(2nm)/thin-MgO/ CoFeB(2.2nm)/CoFe(0.8nm)/Ru(0.85nm)/CoFe(2.5nm)/PtMn(15nm)/cap layers on thermally oxidized Si substrates using magnetron sputtering

*1.7 MΩ•μm^2

SHIOTA *et al.*: THREE-TERMINAL DEVICE FOR REALIZING A VOLTAGE-DRIVEN SPIN TRANSISTOR 4200304

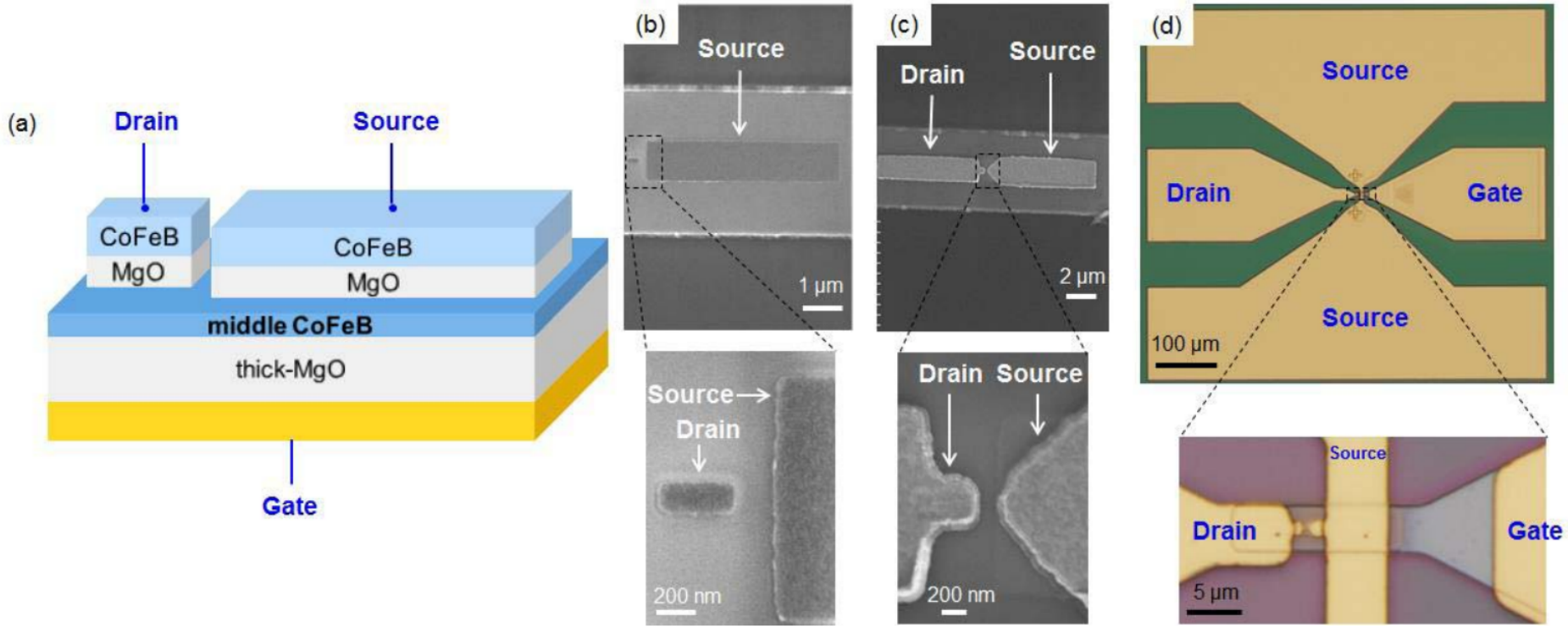

Fig. 2. (a) Diagram of the three-terminal structure we fabricated. (b) Scanning electron micrograph of the drain and source junctions after the third stage of the microfabrication process. (c) Scanning electron micrograph of top electrodes to contact the drain and source junctions after the fourth stage of the microfabrication process. (d) Optical micrograph of the completed three-terminal structure. Insets in (b)–(d): magnified image of the region enclosed in dotted lines.

image from Y. Shiota *et al.*, IEEE TRANSACTIONS ON MAGNETICS **51**, 4200304 (2015)

Spin transistor by anisotropy control - **concept**

- three terminal device with magnetic tunnel junction (MTJ)
- buffer layers/CrB(2.5nm)/thick-MgO*/CoFeB(2nm)/thin-MgO/ CoFeB(2.2nm)/CoFe(0.8nm)/Ru(0.85nm)/CoFe(2.5nm)/PtMn(15nm)/cap layers on thermally oxidized Si substrates using magnetron sputtering

*1.7 MΩ•μm^2

SHIOTA *et al.*: THREE-TERMINAL DEVICE FOR REALIZING A VOLTAGE-DRIVEN SPIN TRANSISTOR 4200304

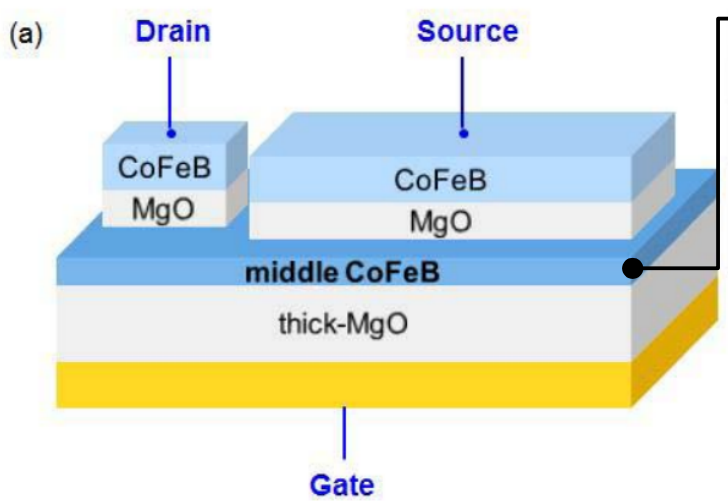

- perpendicular magnetic anisotropy of CoFeB layer is controlled by gate voltage

  the voltage switches the magnetic easy axis from in-plane to out-of-plane direction

  the changes are transformed to the electric circuit via tunneling magnetoresistance (TMR)

Not yet functional: "Although we successfully microfabricated this three-terminal device, we did not observe a distinct change of PMA in the middle CoFeB layer as a result of applying V_{GS}."

Predicted power gain of more than 10^4 (with high load resistance – half of the tunnel junction resistance)

image from Y. Shiota *et al.*, IEEE TRANSACTIONS ON MAGNETICS **51**, 4200304 (2015)

Magnetoelectric charge trap memory - **concept**

- "*a charge-trapping layer integrated into the gate dielectric can provide the missing nonvolatility to the magnetoelectric effect and enhances its efficiency by an order of magnitude*" [23]
- Au(100)/Fe(wedge:0-9ML (≈1.3nm))/ MgO(10nm)/ZrO_2(60nm)/InTO(30nm)

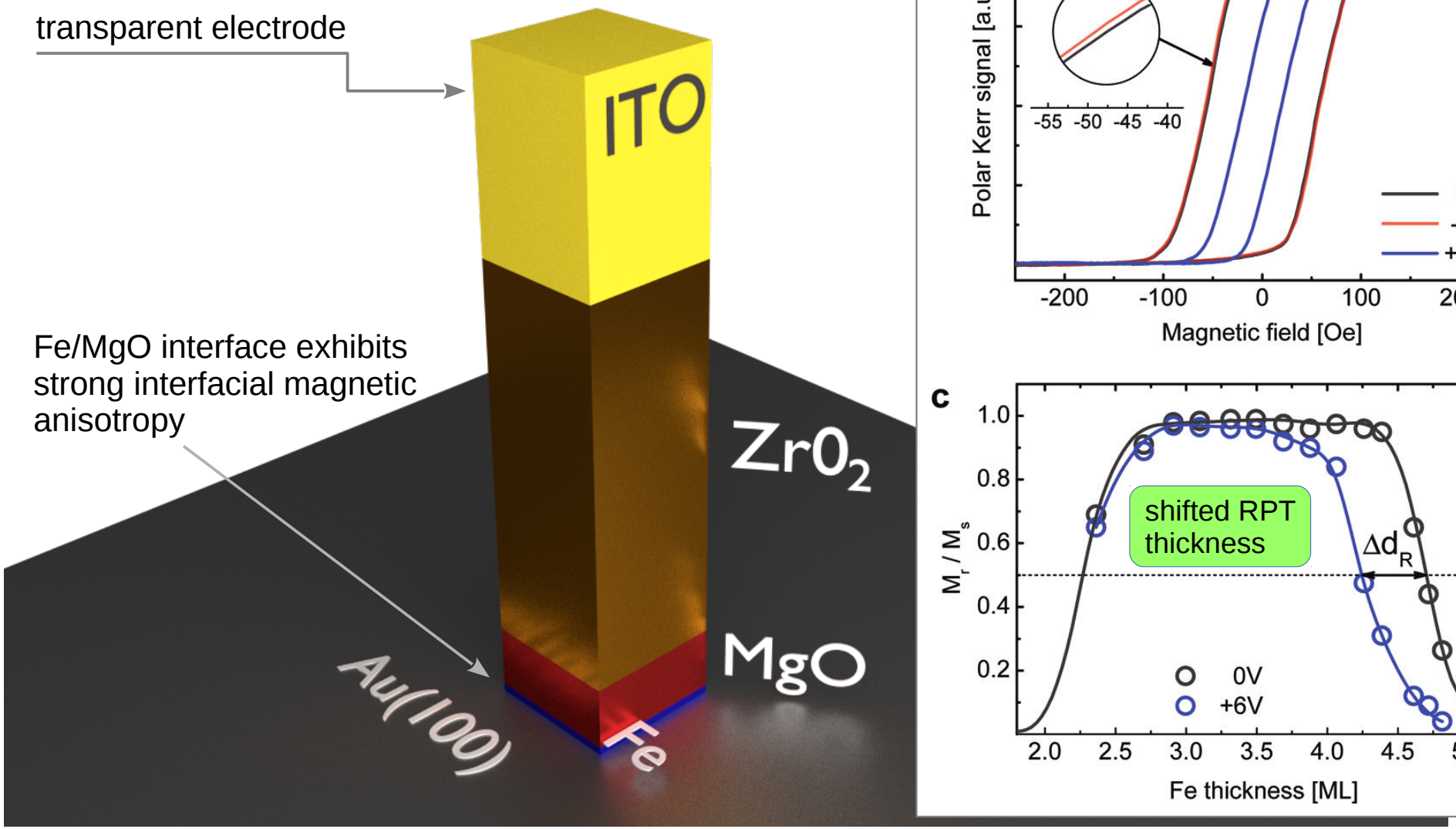

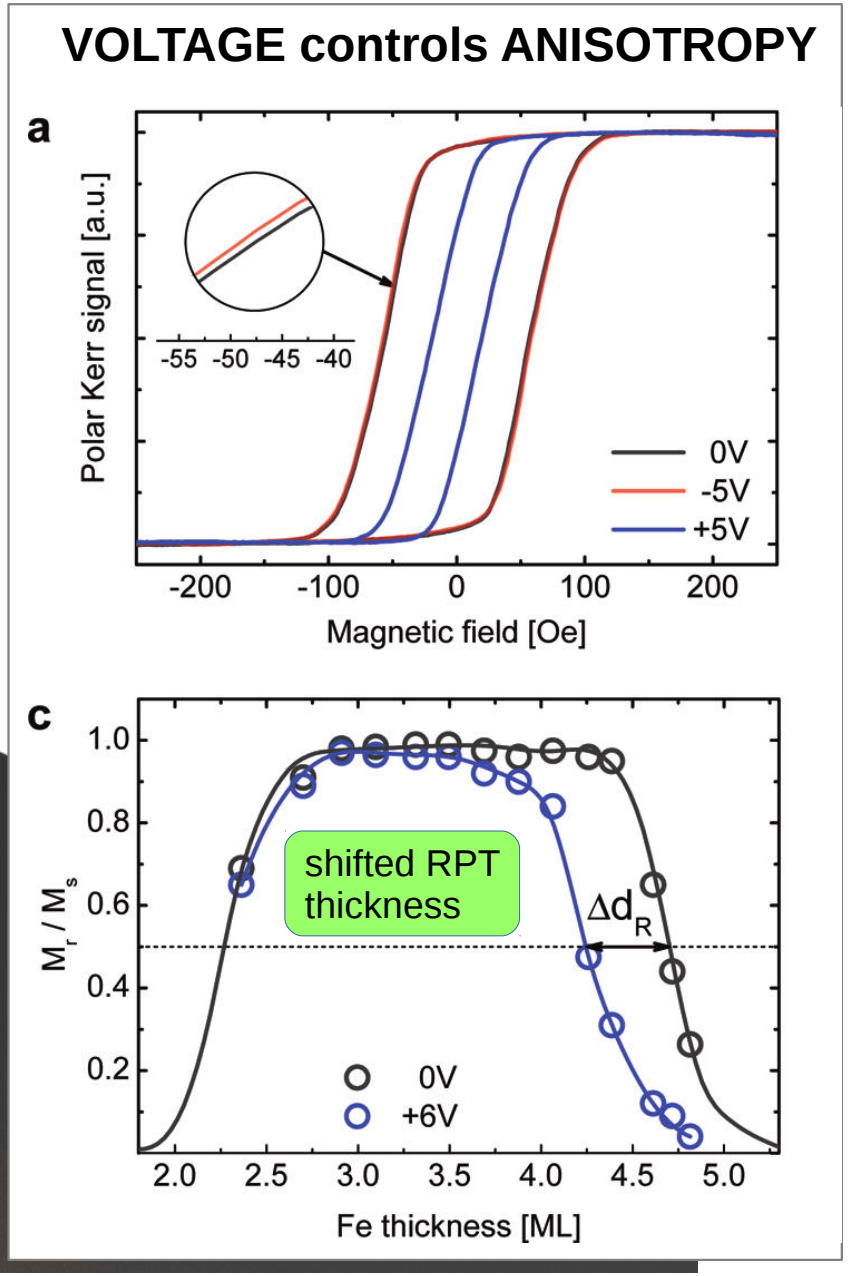

graph from U. Bauer, M. Przybylski, J. Kirschner, and G. S. D. Beach, Nano Lett. **12**, 1437 (2012)

note the small thickness of Fe layers → the screening of electric field in metals

Magnetoelectric charge trap memory - **concept**

- charge retained at the MgO/ZrO_2 interface creates a electric field that disturbs the electron density distribution in Fe layer
- this leads to the changes of the effective perpendicular magnetic anisotropy
- Fe layers of a certain thickness, that would be “above” phase reorientation transition without the presence of the electric field can retain in-plane orientation of the magnetic moments as long as there is enough charge on the interface

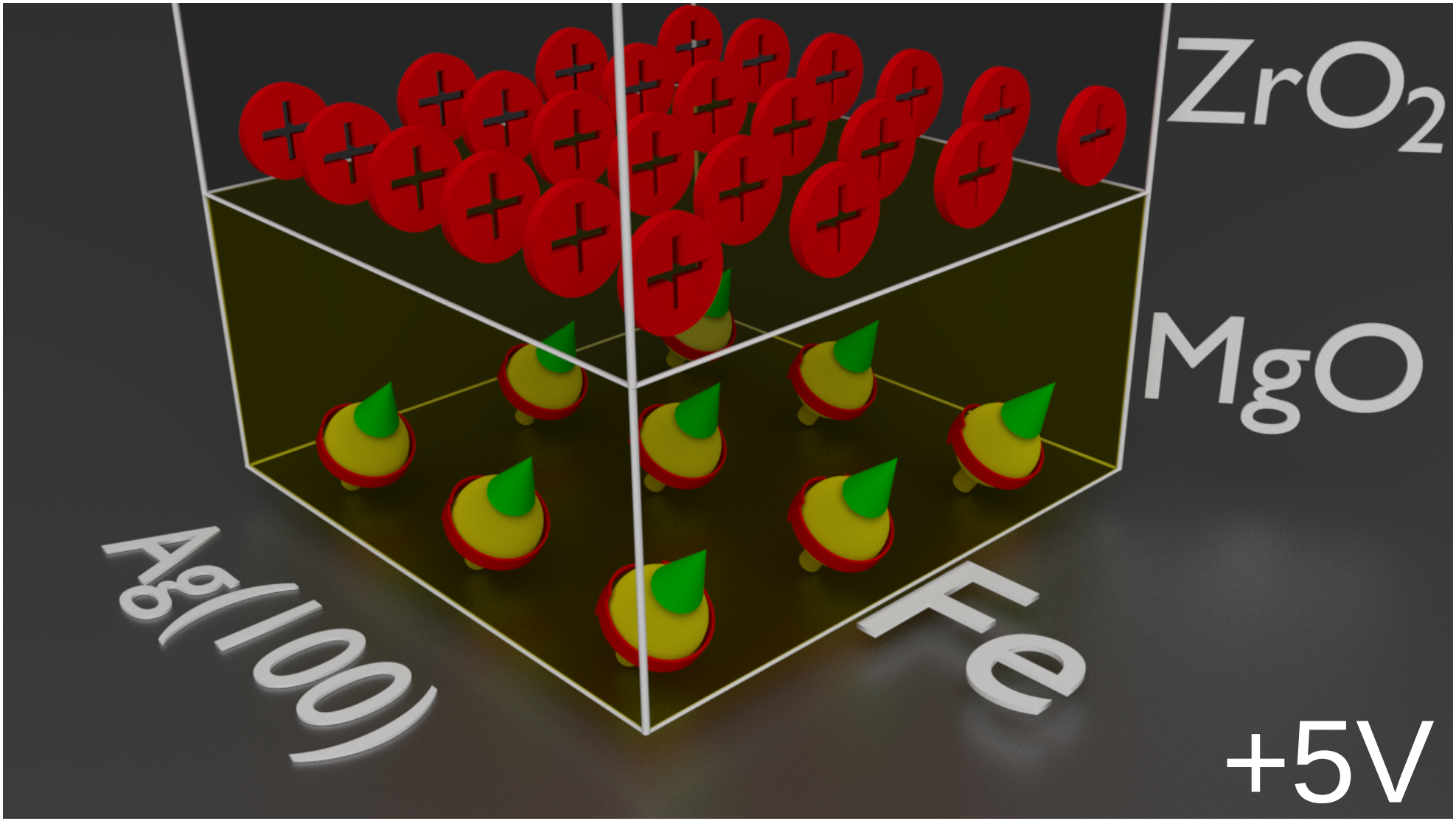

Magnetoelectric charge trap memory - **concept**

- the charges are supplied through an optically assisted process [23]: ITO electrode is a probable source for hole injection
- MOKE measurements show that the changes in magnetic properties (coercive fields, remanence) persist at least 24h after the external bias voltage; **retention times of several days** were observed
- addition of the blocking layer to the dielectric stack ($MgO/ZrO_2/InTO$) should allow, according to the authors, for retention times in excess of **10 years**

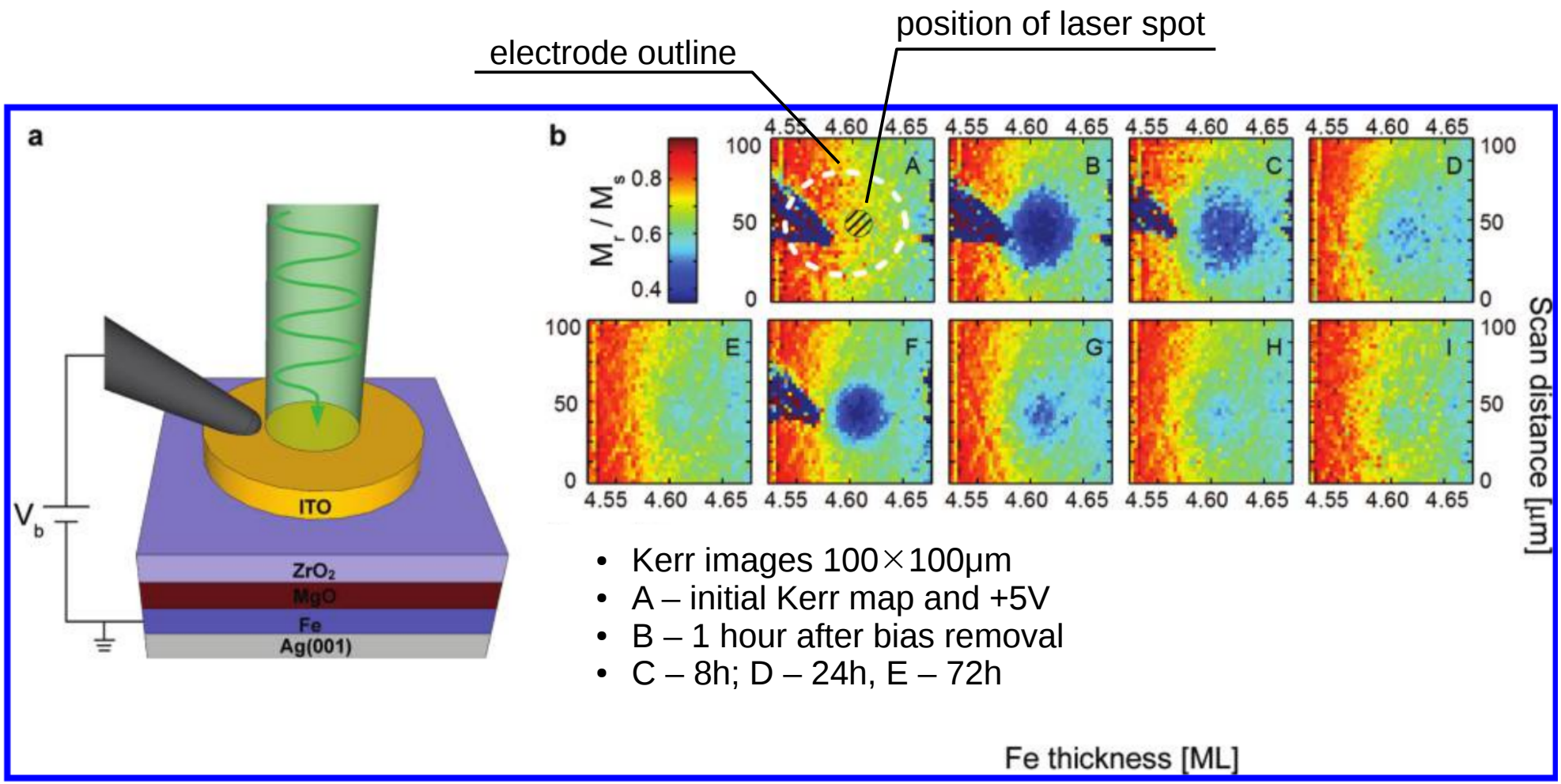

- Kerr images 100×100μm
- A – initial Kerr map and +5V
- B – 1 hour after bias removal
- C – 8h; D – 24h, E – 72h

image (part) from U. Bauer, M. Przybylski, J. Kirschner, and G. S. D. Beach, Nano Lett. **12**, 1437 (2012)

All-Optical Switching (AOS) of Magnetic Tunnel Junctions

- switching of MTJ without magnetic field can be achieved by charge and spin current injection
- the operational speed is limited fundamentally by the spin-precession time to many picoseconds [22]

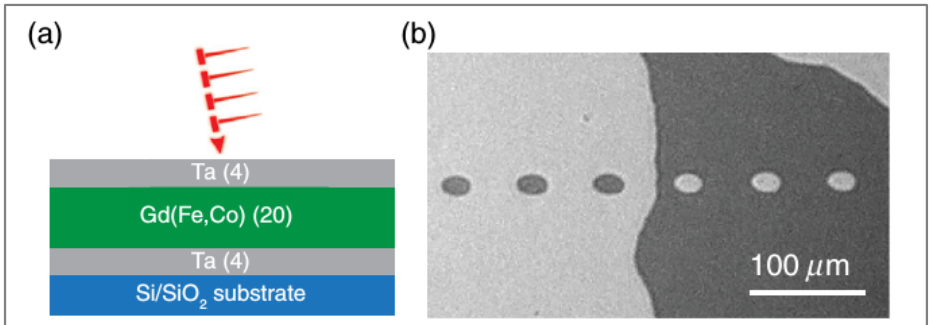

FIG. 1. All-optical switching of Gd(Fe,Co) films. (a) Schematic of Gd(Fe,Co) film structures. Tantalum layers are used as a buffer and capping to prevent film oxidation. (b) The MOKE image of single bubble domains created via AOS by scanning single subpicosecond laser pulses across the boundary between two large magnetic domains in the sample. (c) The coercivity H_c (blue symbols) and saturated magnetization M_s (red symbols) of Gd(Fe,Co) samples versus their Gd composition (x_{Gd}). Samples with Gd composition in the purple-shadowed region (22%–26%) show AOS behavior. The solid lines are used to guide the eyes.

fragment of the image

not patterned

- perpendicularly magnetized Gd(Fe,Co) free layer
- Gd(Fe,Co) cosputtered from $Fe_{90}Co_{10}$ and Gd targets
- 1.55μm wavelength laser; pulse width 400fs; spot diameter 20μm; fluence 5.8mJ/cm^2
- AOS independent of laser polarization (the linear used).
- Laser pulse always reverses the magnetization* (for both orientations of magnetizations – up and down domains)
- Hall effect measurement show almost 100% remanence – rectangular loop

image from Jun-Yang Chen, Li He, Jian-Ping Wang, and Mo Li, Phys.Rev. Appl. **7**, 021001 (2017)
*for possible mechanisms of reversal see M.S. El Hadri *et al.*, Phys. Rev. B **94**, 064412 (2016)

All-Optical Switching (AOS) of Magnetic Tunnel Junctions

- to demonstrate the applicability of the system for AOS in realistic spintronic devices MTJ for TMR readout was designed

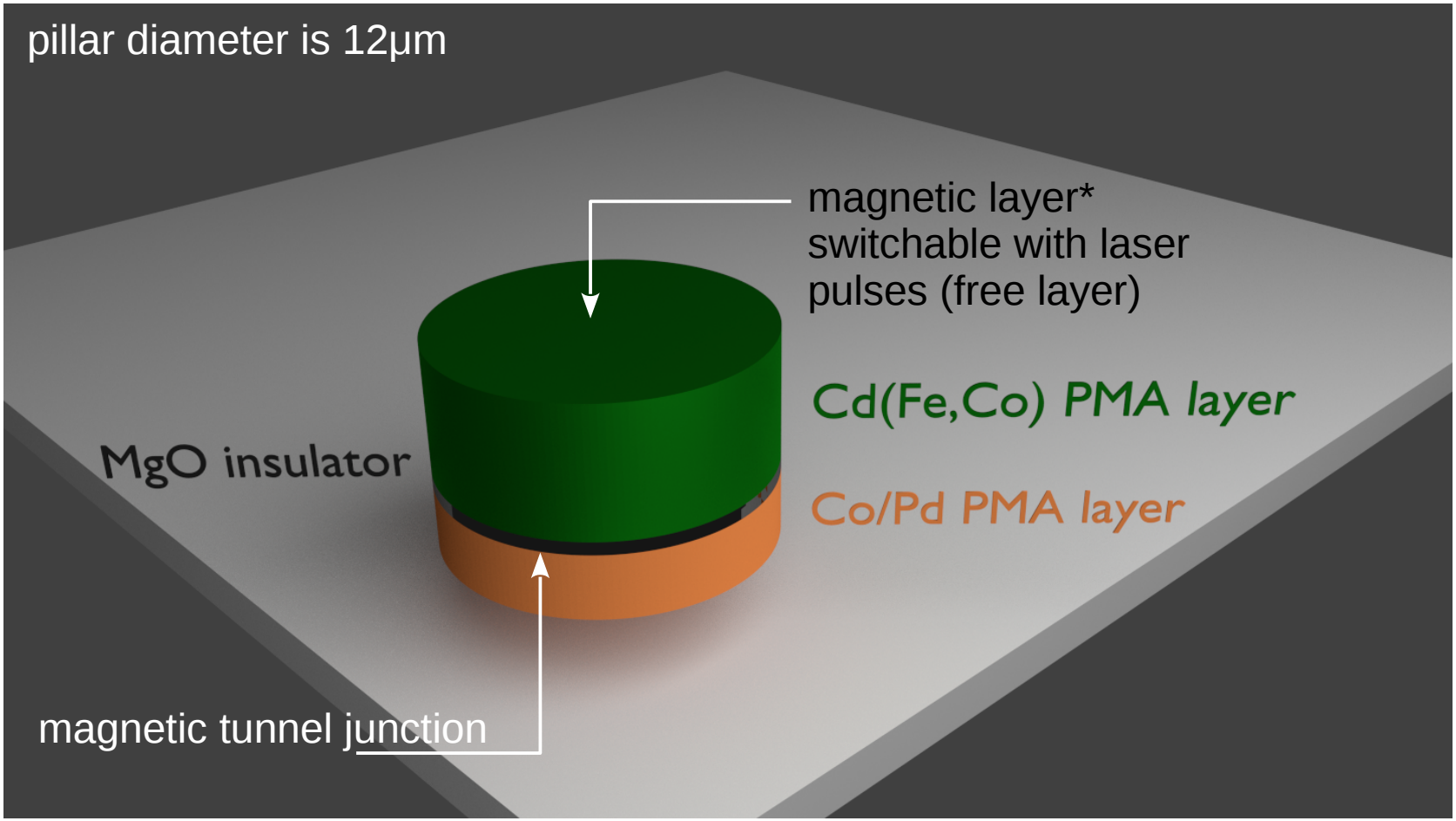

patterned

*$Gd_x(Fe_{90}Co_{10})_{100-x}$ layers for x=22 to 26% display AOS [22]

image adapted from Fig. 3 of Jun-Yang Chen, Li He, Jian-Ping Wang, and Mo Li, Phys.Rev. Appl. **7**, 021001 (2017)

All-Optical Switching (AOS) of Magnetic Tunnel Junctions

- to demonstrate the applicability of the system for AOS in realistic spintronic devices MTJ for TMR readout was designed

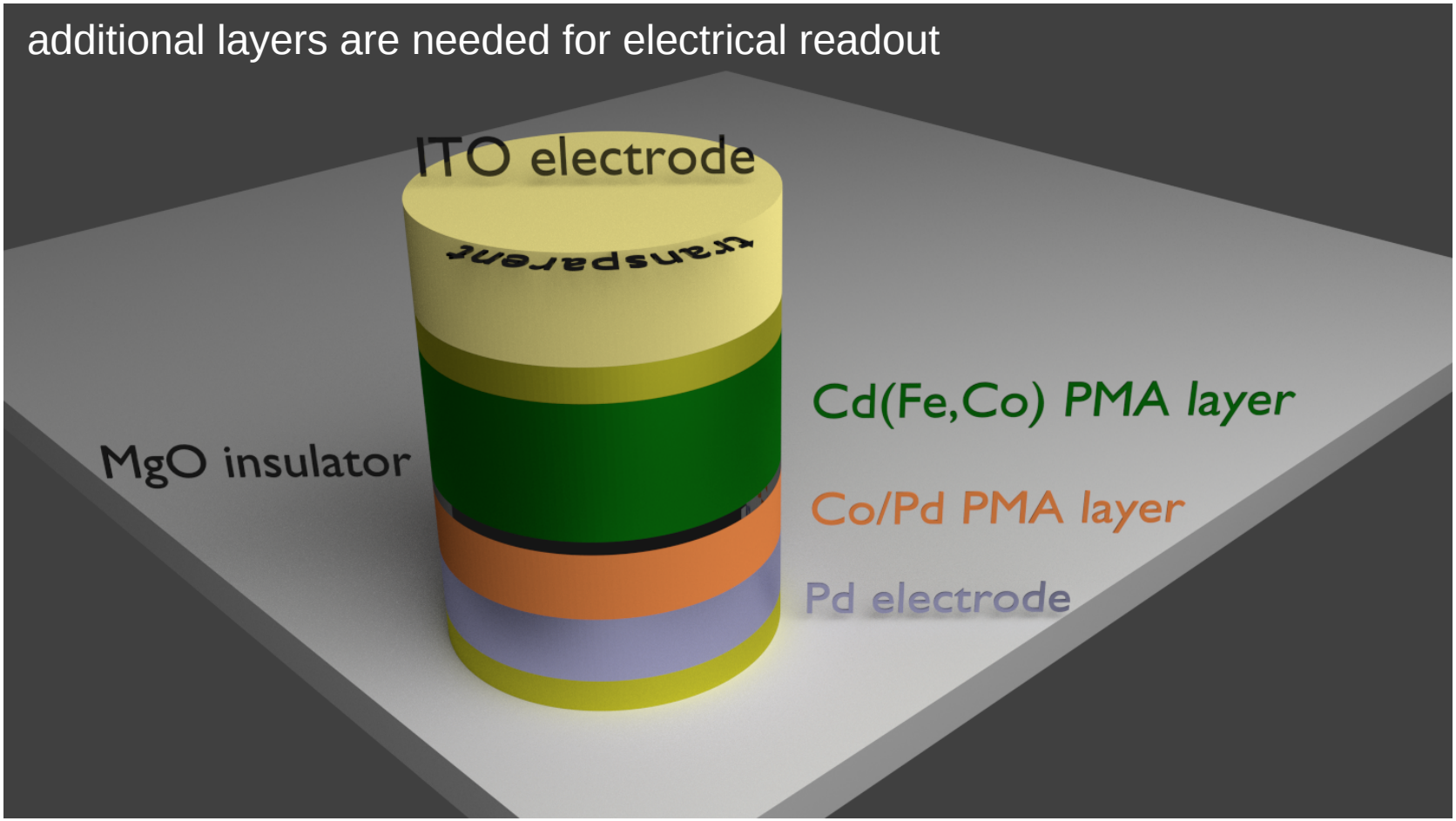

image adapted from Fig. 3 of Jun-Yang Chen, Li He, Jian-Ping Wang, and Mo Li, Phys.Rev. Appl. **7**, 021001 (2017)

All-Optical Switching (AOS) of Magnetic Tunnel Junctions

- to demonstrate the applicability of the system for AOS in realistic spintronic devices MTJ for TMR readout was designed

fragment of the image

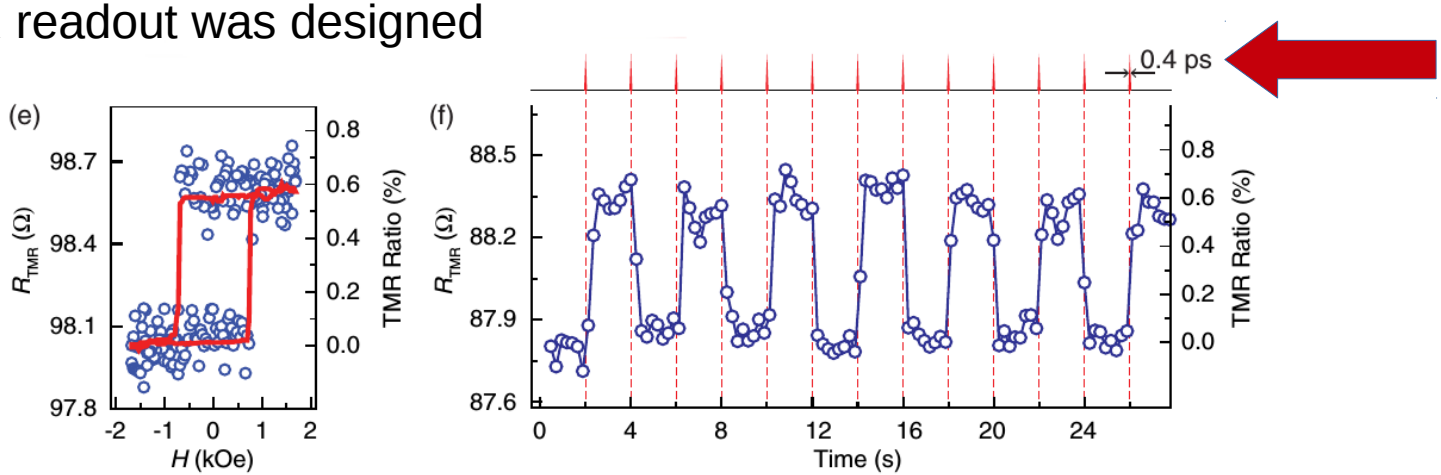

FIG. 3. AOS of an MTJ with subpicosecond single laser pulses without external magnetic field. (a) Schematic of the MTJ structure used in the experiment. (b) Optical microscope image of a typical MTJ device with ITO electrode on the top for TMR measurement. (c), (d) The MOKE images of the MTJ pillar before and after AOS by a single laser pulse, showing the Gd(Fe,Co) layer is completely switched. The pillar diameter is 12 μm. (e) The $R_{TMR}(H)$ minor loop measured by sweeping a perpendicular magnetic field, which switches the Co/Pd layers. The red line is the smoothing of the raw data (open circles). (f) R_{TMR} of the MTJ device measured during AOS by 0.4-ps single laser pulses at 0.5-Hz repetition rate. The changes of R_{TMR} in (e) and (f) have the same value of $\sim 0.6 \pm 0.05\ \Omega$, indicating the Gd(Fe,Co) layer has been completely switched.

- **0.4ps** long laser pulses are able to switch magnetic moments of Gd(Fe,Co) layers
- the picosecond scale switching mode is 2 orders of magnitude faster than other switching methods [22] but one needs laser etc.
- on a Hall effect device it was demonstrated that 1MHz repetition rate; the system **needs more than 10ps to relax to equilibrium**
- the authors argue that the ultimate switching rate of AOS device could be **higher than tens of GHz** as "*subsequent switching can be performed sooner than the system reaches equilibrium*" [22]
- the energy required for switching scales inversely with the device area; "for an AOS device with subwavelength dimensions [...], **femtojoule pulse energy** should be sufficient to switch it." [22]

image from Jun-Yang Chen, Li He, Jian-Ping Wang, and Mo Li, Phys.Rev. Appl. **7**, 021001 (2017)

References

1. T. Dietl H. Ohno, Reviews Of Modern Physics **86**, 187 (2014)
2. Y. Yuan, Y. Wang, K. Gao, M. Khalid, C. Wu, W. Zhang, F. Munnik, E. Weschke, C. Baehtz, W. Skorupa, M. Helm, S. Zhou, Journal of Physics D Applied Physics **48**, 235002 (2015)
3. Z. Bai, L. Shen, G. Han, Y. Ping Feng, *Data Storage: Review of Heusler Compounds* (https://arxiv.org/pdf/1301.5455.pdf)
4. J. M. D. Coey and S. Sanvito, J. Phys. D: Appl. Phys. **37** 988 (2004)
5. I. Galanakis , Ph. Mavropoulos, P. H. Dederichs, J. Phys. D: Appl. Phys. **39**, 765 (2006)
6. C. Felser, L. Wollmann, S. Chadov , G. H. Fecher, S. S. P. Parkin, APL Mater. **3** , 041518 (2015)
7. H-Xi. Liu , Y. Honda, T. Taira , K-ichi. Matsuda , M. Arita , T. Uemura, M. Yamamoto, Appl. Phys. Lett. **101**, 132418 (2012)
8. M. Urbaniak, J-M. Schmalhorst, A. Thomas, H. Bruckl, G. Reiss, T. Lucinski, F. Stobiecki, Physica Status Solidi A **199**, 284 (2003)
9. A. Bonanni T. Dietl , Chem.Soc.Rev. **39**, 528 (2010)
10. J. F. Gregg, I. Petej, E. Jouguelet, C. Dennis, J. Phys. D: Appl. Phys. **35**, R121 (2002)
11. T. Schäpers *Semiconductor Spintronics*, De Gruyter 2016
12. R. Becker, *Theorie der Wärme*, Springer 1964
13. *Compendium of Chemical Terminology (Gold Book)*, International Union of Pure and Applied Chemistry Version 2.3.3 2014-02-24
14. J. Crank, The *Mathematics of Diffusion*, Clarendon Press 1975
15. Th. Schäpers, J. Knobbe, van der Hart, and H. Hardtdegen, Science and Technology of Advanced Materials **4**, 19 (2003)
16. A.J. Schwab, *Begriffswelt der Feldtheorie*, Springer 2013
17. J. Nitta, T. Akazaki, H. Takayanagi, and T. Enoki, Phys.Rev.Lett. **78**, 1335 (1997)
18. H. Akera, H. Suzuura, and Y. Egami, Phys. Rev. B **95**, 045301 (2017)
19. S. Sugahara and J. Nitta, Proceedings of the IEEE **98**, 2124 (2010)
20. Y. Shiota, D. Sekiya, R. Matsumoto, A. Fukushima, K. Yakushiji , T. Nozaki, K. Konishi, S. Miwa, H. Kubota, S. Yuasa, and Y. Suzuki, IEEE TRANSACTIONS ON MAGNETICS **51**, 4200304 (2015)
21. Koji Kita , D. W. Abraham, M.J. Gajek, and D.C. Worledge, J. Appl. Phys. **112**, 033919 (2012)
22. Jun-Yang Chen, Li He, Jian-Ping Wang, and Mo Li, Phys.Rev. Appl. **7**, 021001 (2017)
23. U. Bauer, M. Przybylski, J. Kirschner, and G. S. D. Beach, Nano Lett. **12**, 1437 (2012)
24. M.S. El Hadri, P. Pirro, C.-H. Lambert, S. Petit-Watelot, Y. Quessab, M. Hehn, F. Montaigne, G. Malinowski, and S. Mangin, Phys. Rev. B **94**, 064412 (2016)